



Microbe-induced fluid viscosity variation: field-scale simulation, sensitivity and geological uncertainty

Eric O. Ansah¹ · Hung Vo Thanh¹ · Yuichi Sugai¹ · Ronald Nguele¹ · Kyuro Sasaki¹

Received: 11 November 2019 / Accepted: 5 February 2020 / Published online: 18 February 2020
© The Author(s) 2020

Abstract

This study is intended to expand the scope of microbial enhanced oil recovery (MEOR) simulation studies from 1D to field scale focussing on fluid viscosity variation and heterogeneity that lacks in most MEOR studies. Hence, we developed a model that incorporates: (1) reservoir simulation of microbe-induced oil viscosity reduction and (2) field-scale simulation and robust geological uncertainty workflow considering the influence of well placement. Sequential Gaussian simulation, co-kriging and artificial neural network were used for the petrophysical modelling prior to field-scale modelling. As per this study, the water viscosity increased from 0.5 to 1.72 cP after the microbe growth and increased biomass/biofilm. Also, we investigated the effect of the various component compositions and reaction frequencies on the oil viscosity and possibly oil recovery. For instance, the fraction of the initial CO₂ in the oil phase (originally in the reservoir) was varied from 0.000148 to 0.005 to promote the reactions, and more light components were produced. It can be observed that the viscosity of oil reduced considerably after 90 days of MEOR operation from an initial 7.1–7.07 cP and 6.40 cP, respectively. Also, assessing the pre- and post-MEOR oil production rate, we witnessed two main typical MEOR field responses: sweeping effect and radial colonization occurring at the start and tail end of the MEOR process, respectively. MEOR oil recovery factors varied from 28.2 to 44.9% OOIP for the various 200 realizations. Since the well placement was the same for all realizations, the difference in the permeability distribution amongst the realizations affected the microbes' transport and subsequent interaction with nutrient during injection and transport.

Keywords Artificial intelligence · Viscosity-reducing microbe · MEOR · CMG STARS · Geological uncertainty · Enhanced oil recovery

List of symbols

α Dimensional constant (cross section of the reservoir for one-dimensional reservoir, the thickness of the reservoir for two-dimensional reservoir and 1 for the three-dimensional reservoir)
 λ Mobility
 A Reaction frequency factor
 $avisc_i$ Viscosity correlation factor
 $bvisc_i$ Temperature difference
 C_i Component concentration

E_a Activation energy
 f Weighting factor
 \emptyset Porosity
 ρ Density
 R Molar gas constant
 S_j Saturation of phase
 T Reaction temperature
 t Reaction time
 T_{abs} Absolute temperature related to viscosity
 μ_{L_i} Liquid viscosity
 r_{max} The maximum microbe growth rate
 $\mu_{p,T}$ Water viscosity at specific temperatures and pressures
 x Biomass concentration
 S_o Oil saturation
 S_w Water saturation
 ρ_o Oil density (kg/m³)
 ρ_w Water density (kg/m³)

✉ Hung Vo Thanh
vothanhhung198090@gmail.com

Eric O. Ansah
ansahericbroni@gmail.com

¹ Resources Production and Safety Engineering Laboratory, Department of Earth Resources Engineering, Faculty of Engineering, Kyushu University, Fukuoka, Japan

R_c	Growth and death rate of microorganism (cells/ m^3 s)
R_m	Consumption rate of nutrients by microorganism (kg/m^3 s)
R_p	Production rate of metabolite by microorganism (1/s)
W_c	Cell concentration (cells/ m^3)
W_m	Nutrients' concentration (kg/m^3)
W_p	Metabolites' concentration
Φ_o	Flow potential of oil
Φ_w	Flow potential of water
q_{op}	Production rate of oil (kg/m^3 s)
q_{wi}	Injection rate of water (kg/m^3 s)
q_{wp}	Production rate of water (kg/m^3 s)
GRNN	Generalized regression neural network
MLR	Multiple linear regression
ANN	Artificial neural network
LSSVM	Least square support vector machine

Introduction

Microbes are ubiquitous in almost all global oil reservoirs; normally, they are noted for biodegradation of alkane components of hydrocarbons, thereby changing its physical property (e.g. viscosity). The use of microbes to recover oil has been in existence for over a century, often referred to as microbial enhanced oil recovery (MEOR). MEOR is best suited for depleted and marginal reservoirs, thereby extending the life of oil wells (Lazar et al. 2007). The

environmental and economic advantage of this method makes it the point of interest as per this research. MEOR could be achieved by the reduction in IFT through biosurfactant or bacteria cell, selective plugging by biopolymer, and oil viscosity reduction by biogas, acids and solvents.

The development of detailed MEOR model proves to be challenging not only by the complexity of microbiology but also because of the variety of physical and chemical variables that control the microbe's behaviour in porous media. Table 1 highlights past researches conducted to bring light to MEOR simulation and the respective challenges outlined.

Considering related works regarding MEOR modelling, most neglect fluid viscosity changes by biodegradation and gas production, temperature variation and biogeochemistry (or redox chemistry) of the MEOR process (Table 1). More so, MEOR per gas production is simulated as conventional water-alternating gas flooding. Hence, the need to model and optimizing MEOR considering fluid viscosity and reservoir heterogeneity at field scale.

Since the early 1990s, there have been many reported MEOR projects involving oil viscosity reduction and its accompanying oil recovery increment. The San Andreas well in the USA discovered in 1945 started with the primary drive mechanism, water injection in 1967 and lastly MEOR in 1994. After 19 months of MEOR operations, there were decreased oil viscosity and 10% increase in average daily production (Segovia et al. 2009). In China, the Huaibei field (1995) and Xinjiang field (1996) were both treated to MEOR operation after water injection. After 12 and 24 months of evaluation, the Huaibei field recorded 52% incremental daily

Table 1 Past studies related to microbial enhanced oil recovery (MEOR) modelling

Study/tool	Challenge (s)	Reference (s)
Compositional streamline simulation (using COMSOL and MATLAB)	<ol style="list-style-type: none"> 1. Excludes fluid viscosity modification due to acids/solvents/gases and biomass 2. Excludes temperature effect 3. Unable to simulate real field scenarios such as microbe-induced selective plugging and oil viscosity reduction 4. Neglects redox and chemistry of reactions 	Behesht et al. (2008), Bryant and Lockhart (2002), Desouky et al. (1996), Gianetto (1999), Islam and Farouq Ali (1990), Li et al. (2012), Nielsen (2010), Nielsen et al. (2016), Saito et al. (2016), Shabani-Afrapoli et al. (2011, 2012), Sugai et al. (2014, 2007) and Zhang et al. 1993
UTCHEM	<ol style="list-style-type: none"> 1. Assumes in situ generation of metabolites (surfactant/polymer/gas) by only biodegradation 2. Limited data to validate the model 	Ansah et al. (2018a) and Hosseini-noosheri et al. (2016)
ECLIPSE	<ol style="list-style-type: none"> 1. Microbe plus nutrient transport and their associated effects on reservoir properties cannot be effectively simulated 2. MEOR per biogas mechanism is simulated simply as conventional water-alternating-gas flooding 	Ariadji et al. (2017), Shabani-Afrapoli et al. (2012), Spirov et al. (2014) and Thrasher et al. (2010)
CMG STARS	<ol style="list-style-type: none"> 1. Neglect reaction rate dependent on pressure/phase velocity/effective permeability 2. Limited experimental data to validate microbe-induced selective plugging mechanism 3. Oil viscosity reduction and IFT effects have negligible effects 	Alkan et al. (2016), Ansah et al. (2018b) and Bultemeier et al. (2014)

production and 36% increase for the Xinjiang field, respectively. Both recovered these oil increments because of reduction in oil viscosity (Segovia et al. 2009). Also, in 2004, two producer wells, part of the Peruvian Block X which were under water flooding, were treated by microbe flooding. After 2 months of evaluation, the oil viscosity reduced by 20% but with no significant oil decline rate improvement (Segovia et al. 2009).

The geological heterogeneity of most oil wells is important regarding the optimization of most EOR field applications and its optimization. Unfortunately, geological uncertainty is an inherent characteristic of reservoir models because of the noisy and sparse nature of seismic data, error-prone core measurements and well logs (Yang et al. 2011). Aside other crucial factors—such as rock–fluid properties, injected component and well-operating conditions—a change in reservoir model distribution per heterogeneity significantly influences EOR performance (Al-Mudhafar et al. 2018). Porosity and permeability heterogeneity might influence microbe growth, its transport and metabolism, which will in turn influence oil recovery.

Recently, artificial intelligence (AI), such as artificial neural networks (ANNs), has been adopted to tackle the issues of reservoir heterogeneity and many other applications in the oil industry. For instance, Ahmadi et al. (2014a) and Ahmadi and Chen (2018) demonstrated the accuracy of an ANN model in predicting reservoir heterogeneity comparing real petrophysical data (porosity and permeability data). Also, Ahmadi (2012) developed an ANN model to predict asphaltene precipitation—indicating a high accuracy between ANN model and the experimental precipitation data. Also, ANN was utilized to generate a predictive model to define condensate-to-gas ratio and dew point pressure in retrograded condensate gas reservoirs (Ahmadi et al. 2014b; Ahmadi and Ebadi 2014). Other diverse applications in production technology are: (1) machine learning-based ANN to predict the bottom hole pressure in multiphase flow in

vertical oil production (Ahmadi and Chen 2019); (2) a robust intelligent model to monitor the performance of chemical flooding in oil reservoirs (Ahmadi 2015); (3) performance monitoring of CO₂-foam flooding for EOR and CO₂ storage (Moosavi et al. 2019); and (4) improving CO₂ water-alternating-gas (WAG) combining sequential Gaussian simulation (SGS), co-kriging and ANN to optimize both CO₂ storage and enhance oil recovery (Vo Thanh et al. 2020).

In this study, we show that a compositional model is necessary for MEOR full-field modelling through complicated geological heterogeneity and biogeochemical process. The basic objective was to maintain hydrocarbon component balance so that the recoverable hydrocarbon (both light/heavy) could be determined as a function of the injected microbe and their bioproduct effect. Hence, we modelled microbe-induced fluid viscosity variations by a thermophile, *Petrotoga japonica* sp. (Purwasena et al. 2014a, b). Objectively, we developed a model that incorporates: (1) reservoir simulation of microbe-induced oil viscosity reduction and (2) field-scale simulation and robust geological uncertainty workflow considering the influence of well placement. Adopting the same methodology as Vo Thanh et al. (2020), a robust workflow is presented herein to capture the critical effects of uncertain geological distribution on MEOR performance. In this light, this study is intended to expand the scope of MEOR simulation studies from 1D to field scale focussing on fluid viscosity variation and heterogeneity which lacks in most MEOR studies.

Microbial enhanced oil recovery simulation

We conducted reservoir simulations using both CMG STARS and CMOST. An 8-component model: water, microbe, reproduced microbe, yeast extract, CH₄, CO₂, dead/heavy oil fractions (C17–C20) and light oil fractions (C10–C15) were used to model the dynamic flood data (Table 2).

Table 2 Component composition and fluid properties for simulation

Component	Phase		Molecular mass (gm/gmol)	Property	
	Aqueous	Oleic		Viscosity (cP)	Fraction of reservoir fluid
Water (with 10 g/L NaCl)	x ^a		18.02	0.60	0.993775
Yeast extract	X		18.02	0.60	0.005929
Microbe	X		18.02	0.80	0.000148
Reproduced microbe (microbe ₁)	X		18.02	5.00	0.000148
CO ₂	X	x	44.01	0.001	0.000148
CH ₄	X	x	16.04	0.010	0.000148
Light oil (C10–15)		x	142–212	3.10	0.005929
Dead/heavy oil (C17–20)		x	240–282	7.10	0.993775

^aSymbol ‘x’ represents the presence of a component in a specified phase

Governing equations

The multiphase multidimensional flow through the porous media is represented by the following equations for oil, water, microbe, nutrient and bioproduct, respectively. R_c , R_m and R_p describe the various rates associated with microbe growth, nutrient consumption and bioproduct production (Sugai et al. 2007):

$$\alpha \frac{\partial}{\partial t} (\phi S_o \rho_o) = \nabla \left(\alpha \frac{k_o}{\mu_o} \rho_o \nabla \Phi_o \right) - \alpha q_{op} \quad (1)$$

$$\alpha \frac{\partial}{\partial t} (\phi S_w \rho_w) = \nabla \left(\alpha \frac{k_w}{\mu_w} \rho_w \nabla \Phi_w \right) + \alpha (q_{wi} - q_{wp}) \quad (2)$$

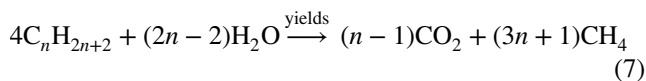
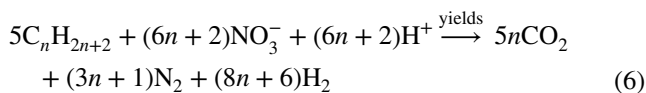
$$\alpha \frac{\partial}{\partial t} (\phi S_w \rho_w W_c) = \nabla \left(\alpha \frac{k_w}{\mu_w} \rho_w W_c \nabla \Phi_w \right) + \alpha \{ \rho_w R_c - W_c (q_{wi} - q_{wp}) \} \quad (3)$$

$$\alpha \frac{\partial}{\partial t} (\phi S_w \rho_w W_m) = \nabla \left(\alpha \frac{k_w}{\mu_w} \rho_w W_m \nabla \Phi_w \right) - \alpha \{ \rho_w R_m - W_m (q_{wi} - q_{wp}) \} \quad (4)$$

$$\alpha \frac{\partial}{\partial t} (\phi S_w \rho_w W_p) = \nabla \left(\alpha \frac{k_w}{\mu_w} \rho_w W_p \nabla \Phi_w \right) + \alpha \{ \rho_w R_p - W_p (q_{wi} - q_{wp}) \} \quad (5)$$

Reaction engineering

Normally, microbe cell grows as an attachment to the alkane, even though growth with n -alkanes is slower (Widdel and Grundmann 2010). All n -alkanes per literature are degraded anaerobically to oxidized CO_2 or completely converted to CO_2 and CH_4 as per the following reactions (Eqs. 6–7), in the presence of sulphate or nitrate source (Widdel and Grundmann 2010).



In CMG STARS, the related reaction of a process in a general form is defined as:

$$n_A \cdot M_A + n_B \cdot M_B + \dots = n_C \cdot M_C + n_D M_D + \dots \quad (8)$$

To this effect, the validation of the reaction and the reaction stoichiometry is done by mass balance, so that moles of each component and energy will be conserved:

$$\sum n_{\text{reac}i} \cdot M_{\text{reac}i} = \sum n_{\text{prod}i} \cdot M_{\text{prod}i} \quad (9)$$

According to Alkan et al. (2016); Bultemeier et al. (2014), Monod's kinetics can be replaced by the following reaction rate for microbe growth as per the CMG STARS equation for chemical reactions:

$$r = F_{\text{Freq}} \cdot e^{(-E_{\text{act}}/R \cdot T)} \prod_{i=1}^{n_c} C_i \quad (10)$$

The exponential factor is responsible for the temperature dependency, and the model calculates a nonzero reaction rate at the initial reservoir temperature (60 °C).

Then, the rate of increase in biomass concentration, x (cells/ml) of AR80 at a time, t (h), and a specific maximum growth rate, r_{max} (1/h), are given as:

$$\frac{dx}{dt} = r_{\text{max}} \cdot x \quad (11)$$

Integrating Eq. (11) solves the bacteria cell number at a time (Sugai et al. 2014):

$$x_t = X_{t-\Delta t} \cdot e^{r_{\text{max}} \cdot \Delta t} \quad (12)$$

In this study, a simplistic model in which the effect of temperature on microbe growth rates was ascertained using the Arrhenius expression. However, the decay rate was not considered primarily because the growth of microbe was assumed to proceed at a maximal rate, which is influenced positively by temperature until impairment (Goldman and Carpenter 1974). With the knowledge that the change of growth with temperature is expressed as activation energy, the maximum growth as a single rate-limiting step was computed as:

$$r_{\text{max}} = A e^{-\left[\frac{E_a}{RT} \right]} \quad (13)$$

where r_{max} is the maximum microbe growth rate (day^{-1}), A is the frequency factor ($-$), E_a is the activation energy (kJ mol^{-1}), R is a molar gas constant ($\text{kJ mol}^{-1} \text{K}^{-1}$) and T is the reaction temperature (K).

Then, the concentration factors are calculated based on their concentration in the respective reference phases as (wherein j is the phase in which component i is reacting, and $X_{i,j}$ represents water, oil or gas mole fractions):

$$C_i = (\theta_f S_j \rho_j X_{i,j})^{\text{Exp}i} \quad (14)$$

Also, per CMG STARS, component (say nutrient) consumption is correlated to bacteria growth by a division factor, F_{div} :

$$r_{\text{div}} = \frac{r}{F_{\text{div}}}; F_{\text{div}} = (1 + A_{xi,j})^B \quad (15)$$

Heretofore, F_{div} is defined per the bacteria mole fraction to model a plateau to which the bacteria amount does not exceed.

The phase viscosity (μ) depends on its respective component viscosity and a weighting factor, f :

$$\ln(\mu_{ij}) = \sum_j [f_{ij} \cdot \ln(\mu_{ij})] \quad (16)$$

where $f_{ij} = X_j$ (specific phase mole fraction) for linear mixing; i = water or oil phase; j = specific component in either water or oil.

Also, the liquid viscosity (μ_{L_i}) in relation to absolute temperature (T_{abs}) follows the equation:

$$\mu_{L_i} = \text{avisc}_i * e^{\left[\frac{\text{bvisc}_i}{T_{abs}}\right]} \quad (17)$$

wherein avisc_i —viscosity (cP) and bvisc_i —temperature difference. Specifying the brine concentration (% NaCl) accounts for the water viscosity ($\mu_{p,T}$) at specific temperatures and pressures as:

$$\mu_{p,T} = \mu \cdot T * f_{p,T} \quad (18)$$

Assuming the incompressible fluid condition, the liquid component (oil or water) viscosity, μ_{L_i} , in the reservoir can be said to be a function of the microbe growth rate, r_{max} (n -alkane biodegradation rate) and mobility, λ .

$$\mu_{L_i} = r_{max} \cdot \lambda \quad (19)$$

where mobility defines the relative permeability with respect to a phase (k_r) over its viscosity (μ):

$$\lambda = k_r / \mu \quad (20)$$

Generation of produced biogas (say CO_2) to reduce oil viscosity is modelled as the partitioning of gas between two phases (oil and water) at different pressures and temperatures via K -value as:

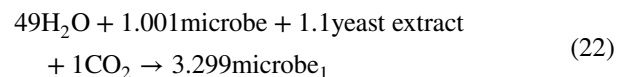
$$K_{\text{CO}_2}^g = \frac{x_{\text{CO}_2(f)}}{x_{\text{CO}_2(l)}} = \frac{x_{\text{CO}_2(l)} + x_{\text{CO}_2(g)}}{x_{\text{CO}_2(l)}} = 1 + \frac{x_{\text{CO}_2(g)}}{x_{\text{CO}_2(l)}} \quad (21)$$

The influence of pressure was considered during the simulation even though it was not observed experimentally. At high biodegradation rate, low oil viscosity and high oil velocity flow, the influence of pressure diffuses.

Various models were considered based on the microbe and substrate reaction and its accompanying metabolite(s) responsible for enhanced oil recovery:

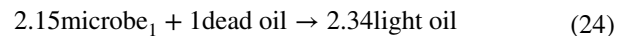
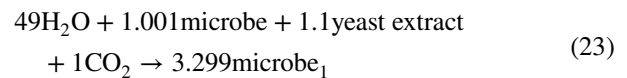
- **Model 1** Microbe growth for biomass increase and possible selective plugging

No geochemical effect and gas production were considered

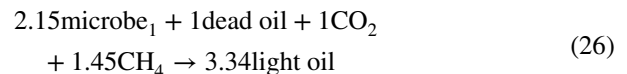
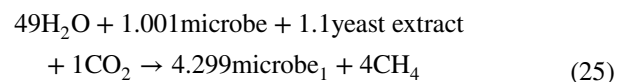


- **Model 2** Microbe growth for biomass increase and oil degradation by the microbe

No geochemical effect and gas production were considered



- **Model 3** Microbe growth for biomass increase and oil degradation by microbe and biogas production. Geochemical knowledge was incorporated.



Furthermore, these assumptions regarding the injected microbe and nutrient into the oil reservoir contended: (1) the reservoir is not unfriendly to the injected microbe; (2) there is no indigenous microbe presence in the reservoir competing for the injected nutrient; (3) limiting the nutrient, yeast extract mostly influences growth and is influenced by temperature, salinity and its quantity injected; (4) both microbe and nutrient adsorption were negligible; (5) all nutrients, metabolites and microbe components are microscopic; hence, transportation is only in the aqueous phase; (6) the only time the system is in equilibrium is when all the nutrients have been consumed. So long as there is nutrient availability, bacteria growth is bound to happen infinitely.

Implementation of reservoir wettability

Considering special conditions (as microbe and nutrient concentration changes, large increases in applied flow velocities, etc.), the assumption is that rock–fluid properties are functioned only of fluid saturation and saturation histories were not enough to accurately describe the observed flow behaviour. In these cases, the relative permeability and capillary pressure were interpolated as functions of phase saturation and/or capillary number. To this effect, two base sets of real permeability and a log of capillary number interpolant were used to history match water flooding and MEOR flooding laboratory experimental data (Fig. 1). Corey's expression was used to attain the endpoints for the relative permeability.

Interfacial tension can change the relative permeability curve. Reduction in the IFT caused the relative permeability

curves to approach linearity (Fig. 1), thereby causing more oil to be displaced during the microbe flooding due to the less frictional force between the oil/water phases. As shown in Fig. 1, the straightening of the curves can also be due to an increase in viscosity of the hydrophilic phase and the decrease in viscosity of the oil phase as bacteria metabolism proceeds. As observed, the intersection points of the two curves (the water saturation equilibrium point between the oil and water relative permeability) decreased from about 63% at the water flooding stage to below 45% during the microbe flooding. Also, the relative permeability to water at maximum water saturation was less than 30% during the water flooding stage but increased sharply beyond 80% for the microbe flooding. Lastly, a gradual decrease in the irreducible water saturation from beyond 56% to less than 20% strongly indicates a shift from an initial water-wet state to a mixed wet state.

The shift in wettability to a mixed wettability state as represented in Fig. 2 can be attributed to the adhesion of the microbe to the oil/rock interface phase, formation of a stable emulsion by the biomass/biofilm of the microbe and the presence of heavier chain *n*-alkanes residual after the biodegradation. Figure 2 highlights three stages responsible for the possible wettability variations. Initially, at point (1) the microbes are in a suspension of biofilm (having the injected nutrient and hydrocarbon substrate) with little adherence to the rock mineral. Assuming the presence of fewer organics (solutes, solvents and acids) in contact with the rock surface, the rock is in a water-wet state, putatively. At point (2), the microbes start settling at the rock–fluid interphase with possible consolidation and reversible adhesion. Finally, at point (3), the microbes

colonize the rock surface, forming a patch of microcolonies and confluent of biofilm on it. Hence, the presence of higher organics amount changes the wettability to a mixed wet state.

The uptake of alkane, liquid plus solid alkanes (above C5), is poorly soluble in water, forming droplets (Eastcott et al. 1988; Wilhelm et al. 1977). In anaerobic alkane degradation, accessing alkanes—the attachment of microbe by hydrophobic cell surface to the alkane phase is concurrent with the production of amphiphilic emulsifying compounds that form micelles (Widdel and Grundmann 2010). Furthermore, attachment of the microbes to the oil surface prevents retrapping, hence increasing mobility and enhanced oil recovery. With this said, MEOR can be more effective in the mixed wet core than on the water wet core, because the residual oil is mostly in interconnected films in mixed wet cores against dislodged drops, which might be in the water-wet cores (Kaster et al. 2012).

Homogeneous 1D simulation

A representative model, as well as input data used in this study, is elaborated in Table 3. The model had one injection well and production well, which were in the first and last blocks, respectively. The injector fluid rate was $2.00746 \times 10^{-06} \text{ m}^3/\text{day}$ for the water flooding stage and then switched to $2.0597 \times 10^{-06} \text{ m}^3/\text{day}$ for both the MEOR stage and post-flush stage. The porosity, permeability, injection scenario and other reservoir and production properties used in this model were as from dynamic flooding experiments (Purwasena et al. 2009, 2014b).

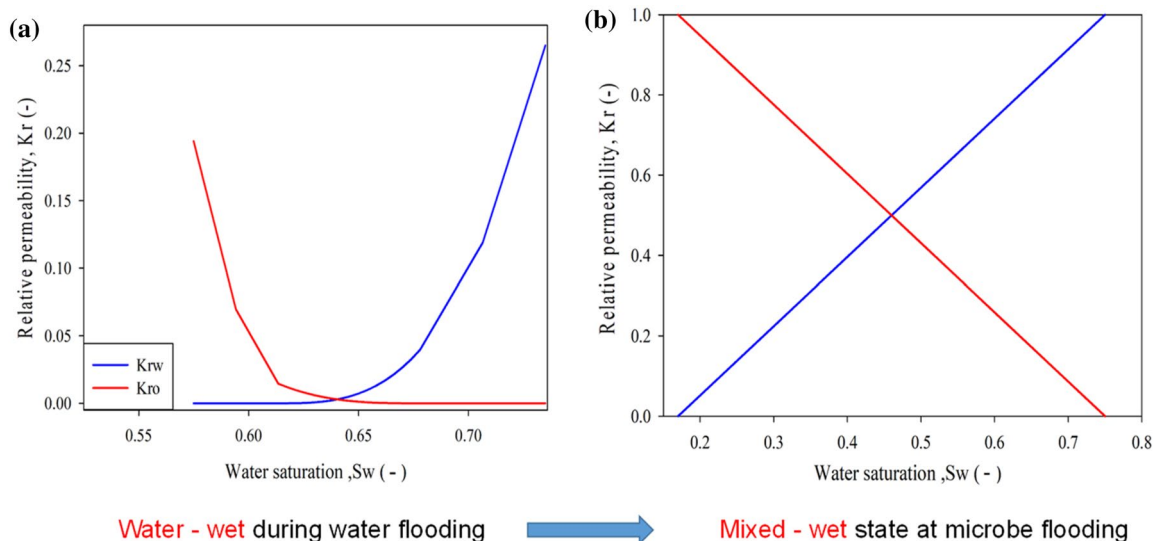


Fig. 1 Oil and water relative permeability curves **a** during waterflooding and **b** during microbe flooding

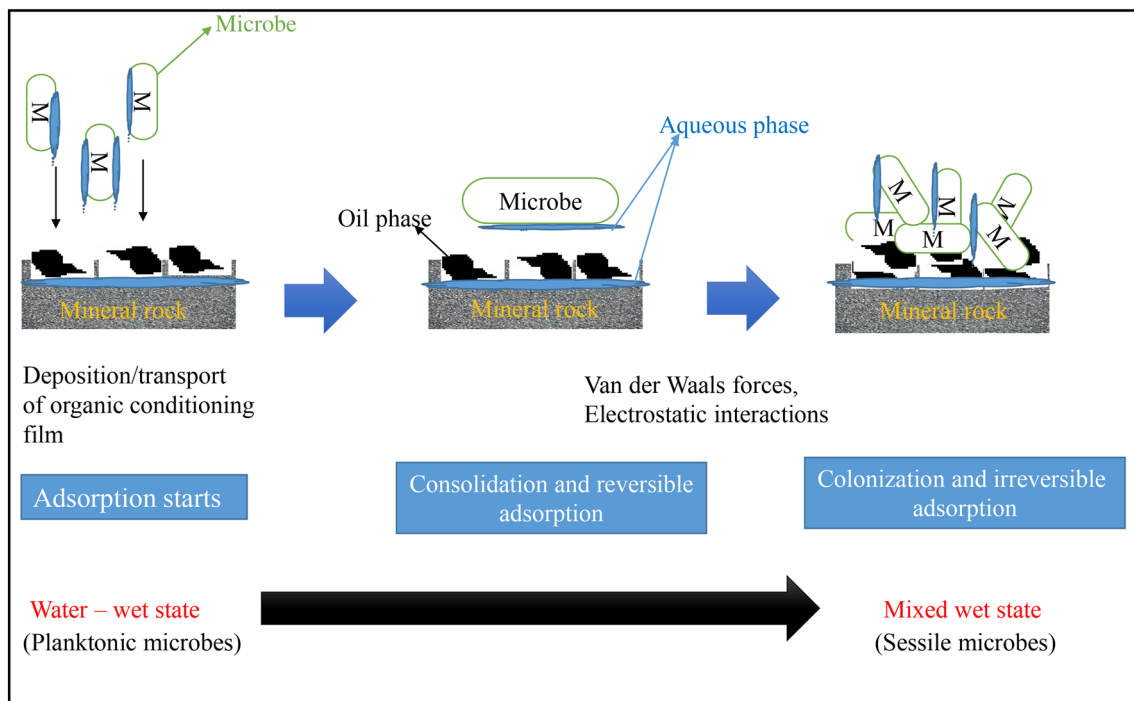


Fig. 2 Schematic diagram for relative permeability changes highlighting three stages of adsorption: suspension of microbes right after injection, reversible adsorption stage at the onset of microbe growth and irreversible adsorption and microbe colonization stage

Experimental data for model validation

A thermophilic (*Petrotoga Japonica* sp.) type of microbe, hereby coded as AR80, was isolated using brine-based and substrate-poor solid culture medium supplemented by CO₂ (Purwasena et al. 2014a). Table 4 highlights the composition of the culture medium and brine used in this study. From experimental studies, AR80 degraded *n*-alkanes under anaerobic conditions at 60 °C as highlighted. They observed the original oil viscosity reduces by almost 70% after 14 days of bacteria incubation with the crude oil (Purwasena et al. 2014b).

A detailed description for optimum controllable conditions (salinity/temperature/pressure/type of crude oil and CO₂ analysis) is reported elsewhere (Purwasena et al. 2014b). AR80 could grow under 3% salinity, 60 °C and 6 MPa. Furthermore, both abiotic and biotic core flooding experiments were carried using AR80 to estimate its injectivity, AR80 growability in a porous medium, and EOR potential of AR80. Crude oil with API of 33°, a viscosity of 7 cP (measured at 60 °C) and a density of 0.958 (measured at 15 °C) were used. Detailed core flooding methodology and results are elaborated elsewhere (Purwasena et al. 2009, 2014b). Experimentally, main oil recovery mechanism was due to oil viscosity reduction, resulting from alkane biodegradation (Purwasena et al. 2009, 2014b). Also, they assumed

Table 3 Simulation input data

Treatment	Treated with microbe
<i>Injection data</i>	
PV injected during pre-flush with brine and yeast extract	3.0
PV injected during culture medium with the microbe	3.0
Shut-in period (days)	14
PV injected during the post-flush with brine	2.5
<i>Core flood data</i>	
Reservoir size (cm)	8 × 1 × 1
Number of grid blocks	40 × 1 × 1
Grid block size (cm)	0.2 × 1 × 1
Initial reservoir temperature (°C)	60
Initial reservoir pressure (MPa)	6
Pore volume (mL)	16.48
Porosity (%)	20.65
Absolute permeability (mD)	300
Oil viscosity at 60 °C (cP)	7
Initial water saturation (%)	61.3
Residual oil saturation (%)	38.7

a decrease in mobility ratio from 10 to 6 and increase in sweep efficiency from 0.830 to 0.90 in the core (Purwasena et al. 2009, 2014b).

Microbial growth rate modelling

Figure 3 highlights the bacteria growth rate and its relation to oil viscosity reduction. As per the Arrhenius expression elaborated in Fig. 3a, the exponential microbe growth phase was modelled—a satisfactory agreement between the model and data set is reported. Figure 3b shows the microbe growth against viscosity reduction. The experimental data are as per static bottle test (contacting the microbe with the hydrocarbon—oil), whereas dynamic simulations were conducted to model the experimental data under the same conditions. As the microbe growth proceeds, oil viscosity reduces radically from initial 26.6 to 17.6 cP (for the model) and 16.6 cP (per experiment). The model was run for only 15 days to ascertain this effect at a higher fraction of light oil, CO₂ and CH₄ by increasing their stoichiometry coefficients (Fig. 3b).

Reservoir simulation: assessment of model types

Figure 4a shows the oil recovery (%) investigated for each model scenario. The increase in oil recovery for all the investigated cases can be related to oil displacement as a function of oil viscosity. As indicated, the oil viscosity decreases from the upstream (injector) to the downstream (producer), accompanied by a mobility increase for heightened oil recovery (Fig. 4b). Fluid acceleration is transferred from one fluid layer to another. It is inferred that the total

oil recovered after brine and microbe flood for model type 3 was the highest comparing the two other cases. In the first (1st) case, the biomass cells of the microbe can be said to have played the main role of oil viscosity reduction (Fig. 4b).

However, in models 2 and 3, contributions by the biomass cells plus biogenic CO₂ and CH₄ induced the oil viscosity reduction. As per this, it can be concluded that incorporating the idea of nutrient speciation and rock–fluid/fluid–fluid interaction to produce CH₄ and CO₂ leads to heightened oil recovery for both the brine and microbe flood stages. Of the three model types, model type 1 had more viscous oil left behind after 90 days (end of the microbe flooding process) (Fig. 4b). An increase in oil viscosity reduction ensured more oil recovery resulting from increased mobility to the production well. Therefore, model type 3 was adopted for history matching of the experimental data.

Figure 5 highlights the history match results for the laboratory experimental data. Due to the intuitive and qualitative nature of manual history match, automatic history match with a quantitative approach was conducted (Fig. 5). Automatic history match (HM) was performed to have a range of plausible HM solution other than one precise HM results. The automatic history match shows improvement in the matching quality and an average history match error of less than 3%.

Table 4 Ionic composition of brine used for enrichment (of AR80) culture medium a [6]

Na ⁺ : 3075	K ⁺ : 30	Ca ²⁺ : 5	Mg ²⁺ : 3	NH ₄ ⁺ : 15
Cl ⁻ : 2500	I ⁻ : 1.5	HBO ₂ ²⁻ : 250	HCO ₃ ³⁻ : 4000	
T-Fe: 2	Acetic acid: 4.3	Formic acid: 2.2	Lactic acid: <0.1	Propionic acid: <0.1

Composition is given in ppm

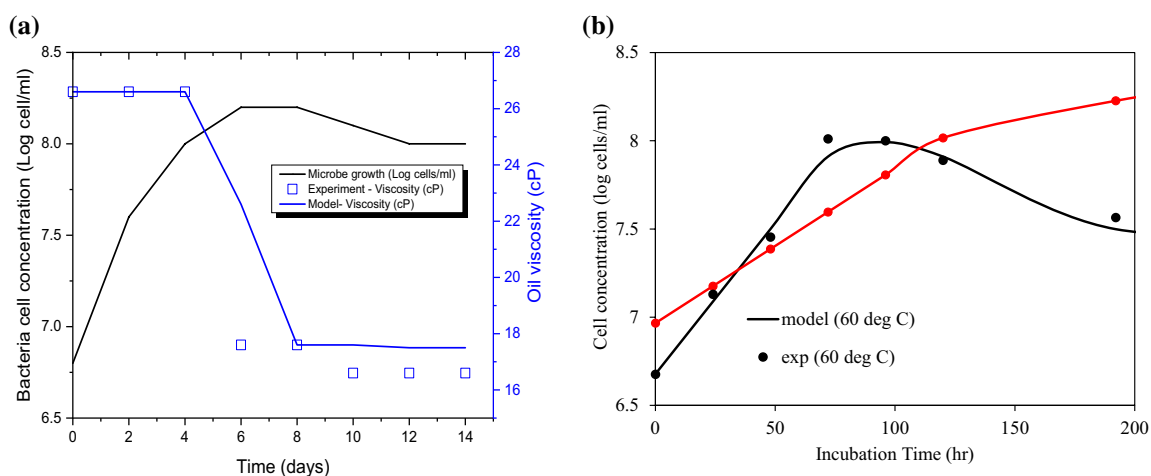


Fig. 3 History matching for **a** oil viscosity reduction and microbe growth rate and **b** microbe growth rate per temperature variation

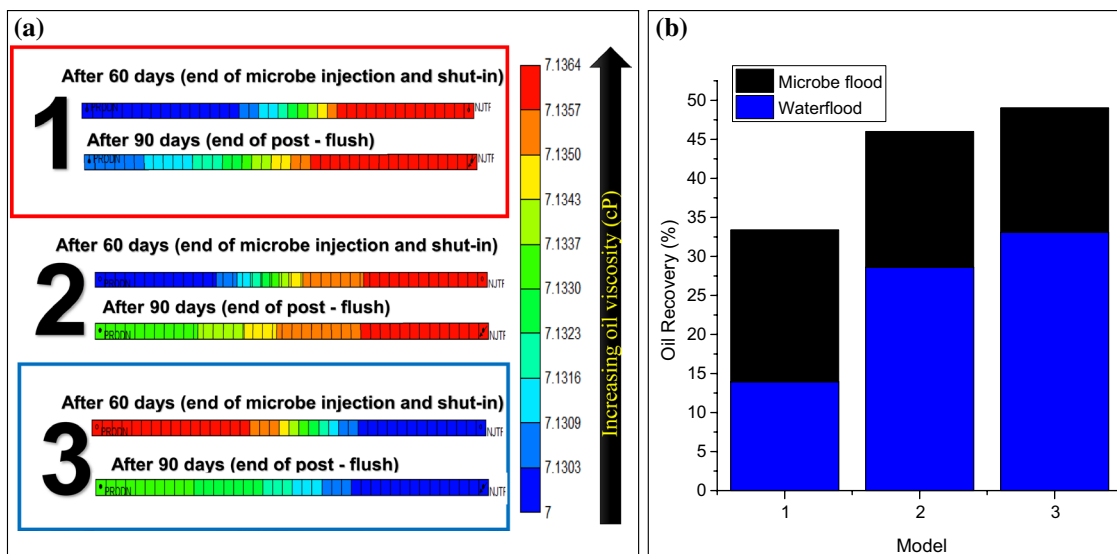


Fig. 4 a Oil viscosity variation per the different models and b oil recovery (%) per the different models considered

Component concentration effect on oil viscosity reduction

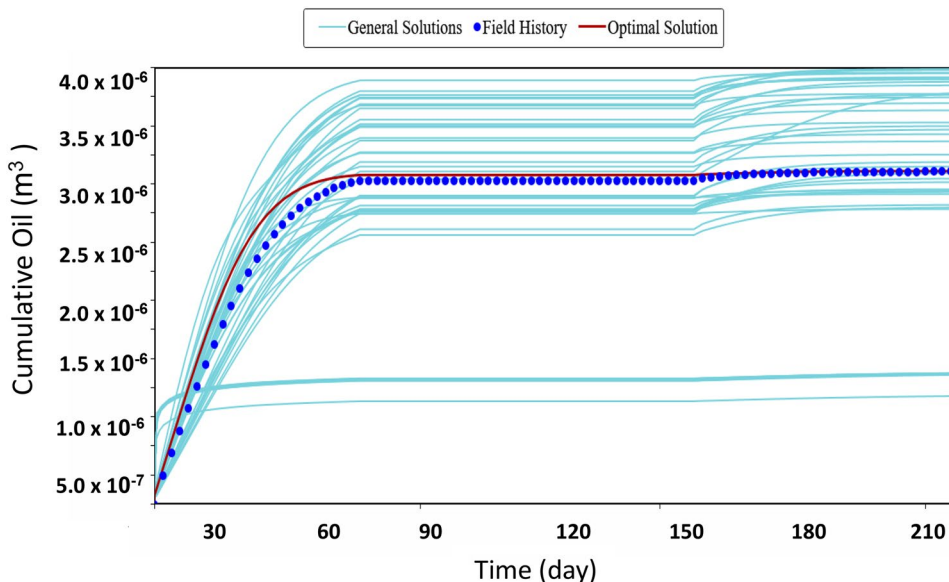
Throughout this whole study, it has been established that oil viscosity reduces per alkane biodegradation to improve oil recovery. In this section, elucidation on the phenomenon behind component concentration effect on fluid viscosity variation depicted by the sensitivity assessment is discussed.

We investigated the effect of the various component compositions and reaction frequencies on the oil viscosity and possibly oil recovery (Fig. 6a, b). For instance, the fraction of the initial CO₂ in the oil phase (originally in the reservoir) was varied from 0.000148 to 0.005 to promote the reactions

in case study 3, and more light components were produced (Fig. 6b). We realized this could also be achieved by changing the stoichiometric coefficient of the components. It can be observed that the viscosity of oil reduced considerably after 90 days of MEOR operation from an initial 7.1–7.07 cP and 6.40 cP, respectively (Fig. 6b).

Also, the higher amount of lower weight *n*-alkane originally present in the reservoirs (C10–15) ensured high biodegradation rate and less residual viscous oil. This is so because microbes are known to be able to degrade easily aliphatic chains compared to aromatic or heavier *n*-alkane chains.

Fig. 5 Oil recovery—history match against experimental data (blue dot)



Biomass influence on water viscosity variation

The water viscosity increased from 0.5 to 1.72 cP after the microbe growth and increased biomass/biofilm. It was observed that as the biomass population increased with increasing biomass viscosity (from 5 to 10 cP), there was a correlated increase in the water viscosity (Fig. 7). Increments in the water viscosity can be said to have improved sweep efficiency of the reservoir to recover residual oil. Figure 7 shows the frontal advancement of the reproduced microbe (mass fraction of aqueous phase) in the homogeneous core model. Increasing the biomass population and subsequent biomass viscosity led to selective plugging of preferential areas of the reservoir, ensuring fewer thief zones in the reservoir, because microbes are known to exist in water droplets in the oil phase or even in water film surrounding rock mineral grains (Meckenstock et al. 2014).

Artificial Neural Network for geological modelling

First, a realistic geological model was created by considering all the crucial factors, including facies, distribution porosity and permeability. The model is a fluvial sandstone reservoir that has two different facies: fluvial channel sand and floodplain shale. The facies model was distributed using

a geological package based on object-based modelling using the parameters as shown in Table 5. The distribution of the two facies modelled is presented in Fig. 8. The reaction engineering of the 1D simulation as presented above was upscaled assuming an isothermal condition by fixing the enthalpy of reaction at zero. All other conditions unless otherwise mentioned were kept unchanged.

Sequential Gaussian simulation (SGS), co-kriging and artificial neural network (ANN) were used for the petrophysical modelling. The ANN was employed to train the seismic attributes and well log to predict porosity and permeability models. SGS and co-kriging were adapted to combine the facies model and ANN prediction cube into one single model. Next, the drill stem test matching was performed to validate the accuracy of the model for further investigation (Vo Thanh et al. 2019a, b). Figure 9 depicts the reasonable porosity and horizontal permeability models for this work.

Performance of the ANN model

This section highlights the performance of the ANN model. The seismic data and well-log data were represented as input layers in the ANN model, whilst porosity and permeability were the output layers in the training framework. The seismic data were created using four different seismic attributes: signal-processed attributes, complex trace attributes, structural attributes and stratigraphic attributes. Then, the

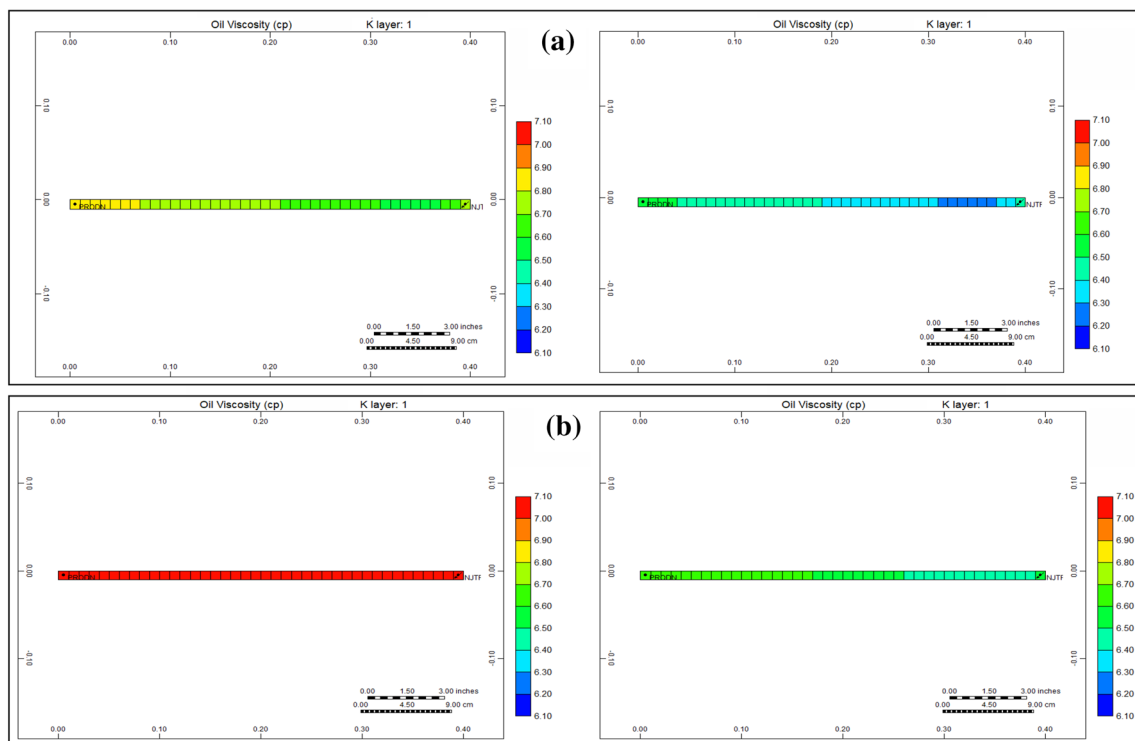


Fig. 6 Oil viscosity variation per component content: **a** light oil fraction and **b** CO₂ fraction. Start of simulation (left); End of simulation (right)

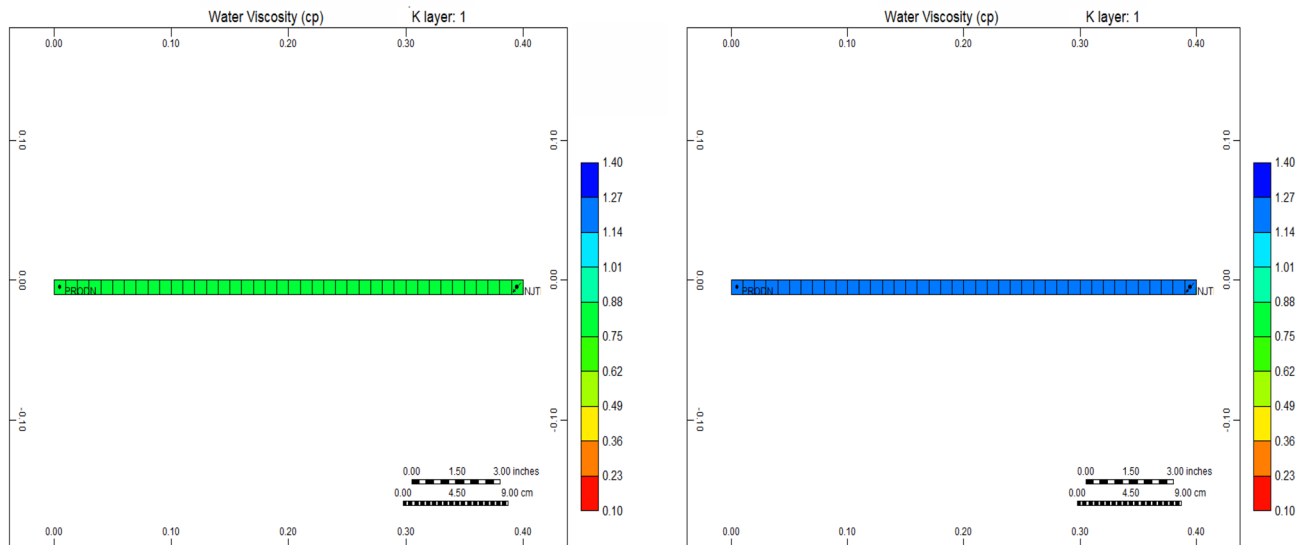


Fig. 7 Water viscosity variation per biomass increase. Start of simulation (left); End of simulation (right)

Table 5 Input parameters used in lithofacies modelling

	Min	Mean	Max
Orientation	45		
Channel amplitude (m)	600	700	800
Channel wavelength (m)	1600	2000	2400
Channel width (m)	350	500	650
Channel thickness (m)	35	50	65

ranking of the seismic attributes was performed using ANN MATLAB toolbox. The performance of the developed ANN model was based on training, validation and blind testing data set. The correlation factor and mean square error (MSE) were then utilized to evaluate the quality and accuracy of the developed ANN model.

After repeated trails training, it was indicated that the neural network model with eight hidden neurons in the

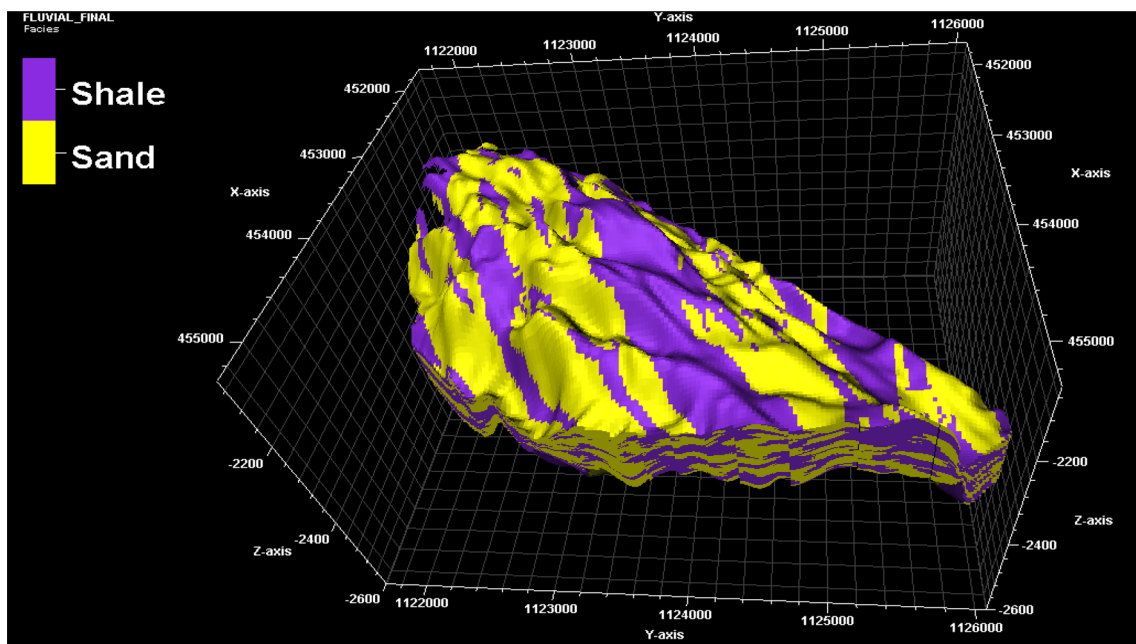


Fig. 8 Facies model in this study

hidden layer obtained the excellent performance for the porosity and permeability with a validation MSE value of 3.96×10^{-5} and 2.78×10^{-4} , respectively.

The illustration of the ANN network is depicted in Fig. 10. For porosity-type ANN model, the training process was achieved at 35 epochs with a validation MSE of 3.96×10^{-5} (Fig. 11a). Figure 11b depicts the best validation performance and the regression plots of ANN porosity model for training, validation and blind testing groups, respectively. The predictive porosity model matches so well to the well-log porosity values for all training, validation and blind testing groups as can be observed in their correlation factor (R) of 0.946, 0.988 and 0.994 for training, validation and blind testing, respectively.

Similarly, the performance and regression plot of ANN permeability model are highlighted in Fig. 12. For permeability ANN model, the training process was successfully truncated at 86 epochs with a validation MSE of 2.78×10^{-4} . Also, the ANN permeability model fits so well to the well-log permeability values for all training, validation and blind testing groups as can be investigated in their correlation factor (R) of 0.989, 0.983 and 0.978 for training, validation and blind testing, respectively.

Comparison between the developed ANN model and existing artificial intelligence studies

There are many previous studies focussing on the prediction of porosity and permeability using artificial intelligence (AI). Table 6 points out some of these related studies, and the comparison between those AI models and this study. According to Table 6, it can be observed that the prediction

accuracy of this study significantly differs from several existing works. In that, the developed ANN model of this study outperforms other AI models. The main reason is because the current ANN model uses less number of neurons in the hidden layer as compared to the previous AI model. Regarding the results in terms of error and efficiency, the ANN models in this study are demonstrated to be more suitable for prediction of porosity and permeability due to higher R^2 and low MSE compared to previous AI models.

Field-scale simulation and optimization

In this section, full-field simulation and optimization are conducted to give insight into recovery efficiency under various drive mechanisms (comparing MEOR and water flooding) and also to show variations through complex reservoir heterogeneity and better tracking of injected microbe (Fig. 13). For field-scale implementation, we set the activation energy to zero to assume isothermal reactions and quicken the MEOR growth and metabolism reaction. When the reaction front sweeps through the reservoir, a certain amount of oil serves as a carbon source for microbe growth. The rest of the mobile oil gets pushed further downstream through viscosity reduction.

Afterwards, multiple geological realizations were generated and ranked to select nine representative realizations to capture geological uncertainties. The geological uncertainty assessment was performed by including the nine quantiles of ranked geostatistical realizations (P10, P20, P30... and P90) for porosity, permeability and anisotropy ratio. To capture the geological uncertainties, 200 porosity and permeability

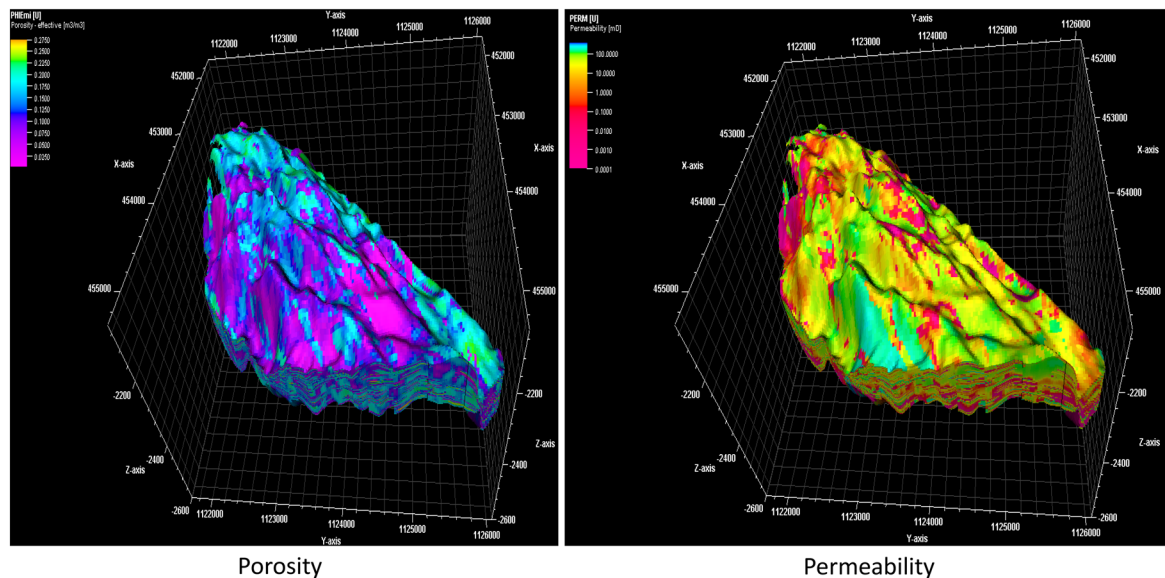


Fig. 9 The reasonable porosity and horizontal permeability models for this study

Fig. 10 The architecture of neural network for this work

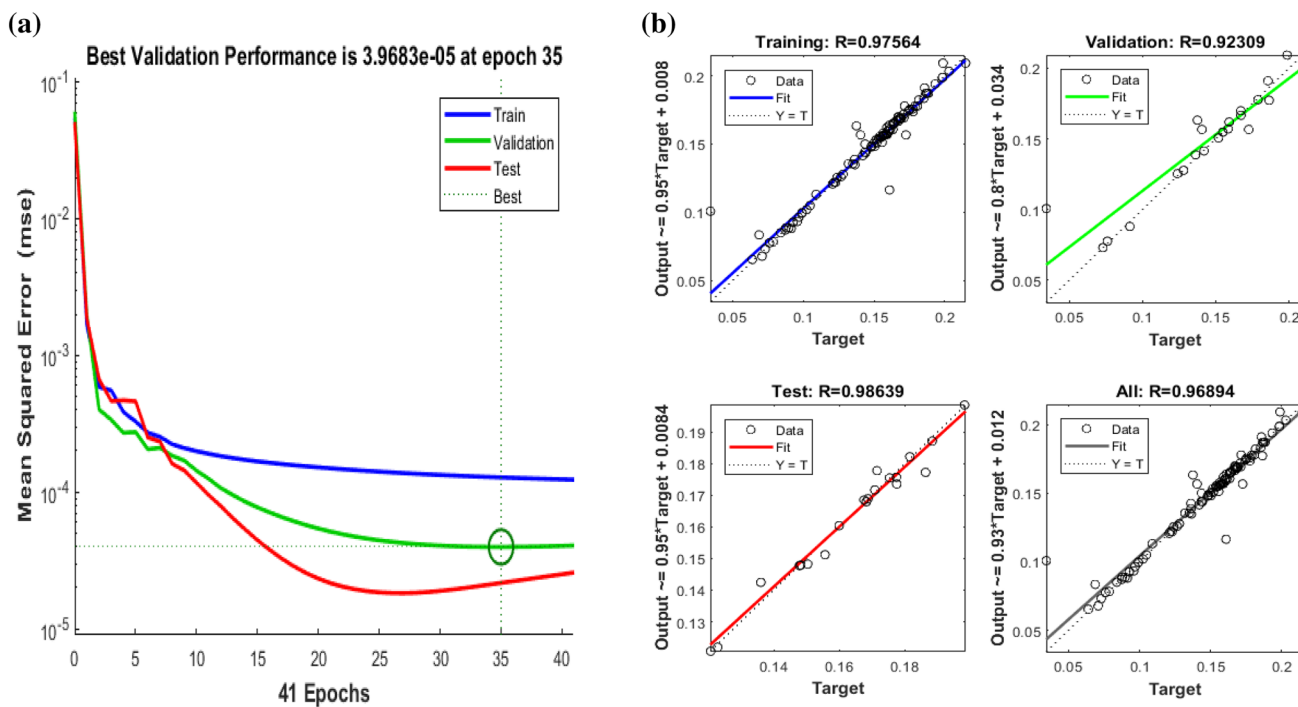
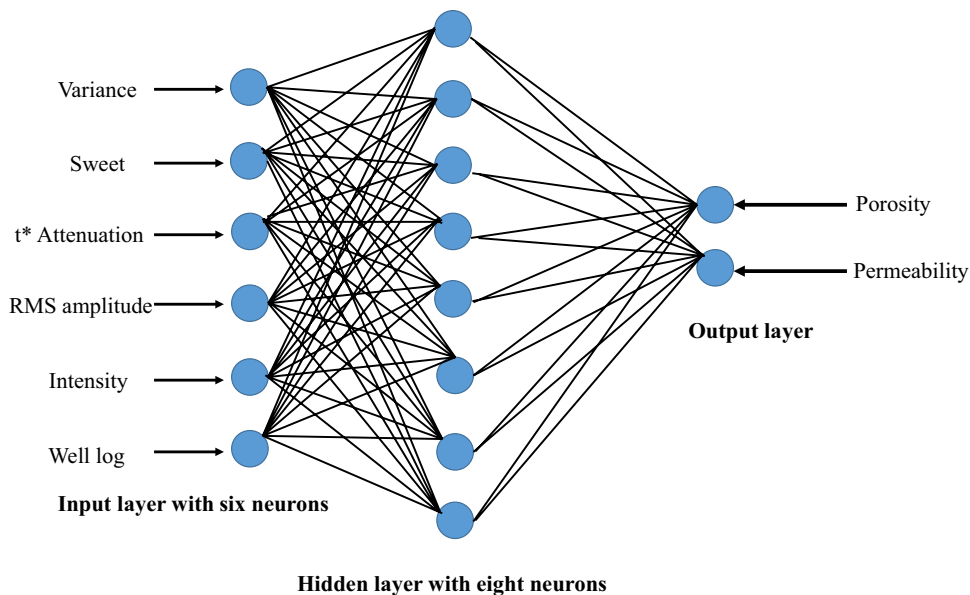


Fig. 11 Performance and regression plot of porosity ANN model

realizations were generated honouring geological constraints using sequential Gaussian simulation. Since it was difficult to simulate all these geological realizations in the optimization process due to limited computational resources, ranking, based on the oil recovery factor, was considered for permeability and pore volume for porosity to select the P10, P20, P30, ..., and P90 that represent the overall geological

uncertainties. All these permeability models were evaluated in the MEOR reservoir model for the ranking process within 25 years of production.

Figure 14a shows the histogram of the generated 200 porosity realizations based on the pore volume. Also, this figure illustrates the selected nine quantiles (P10, P20, P30, ..., and P90) that were obtained based on the cumulative

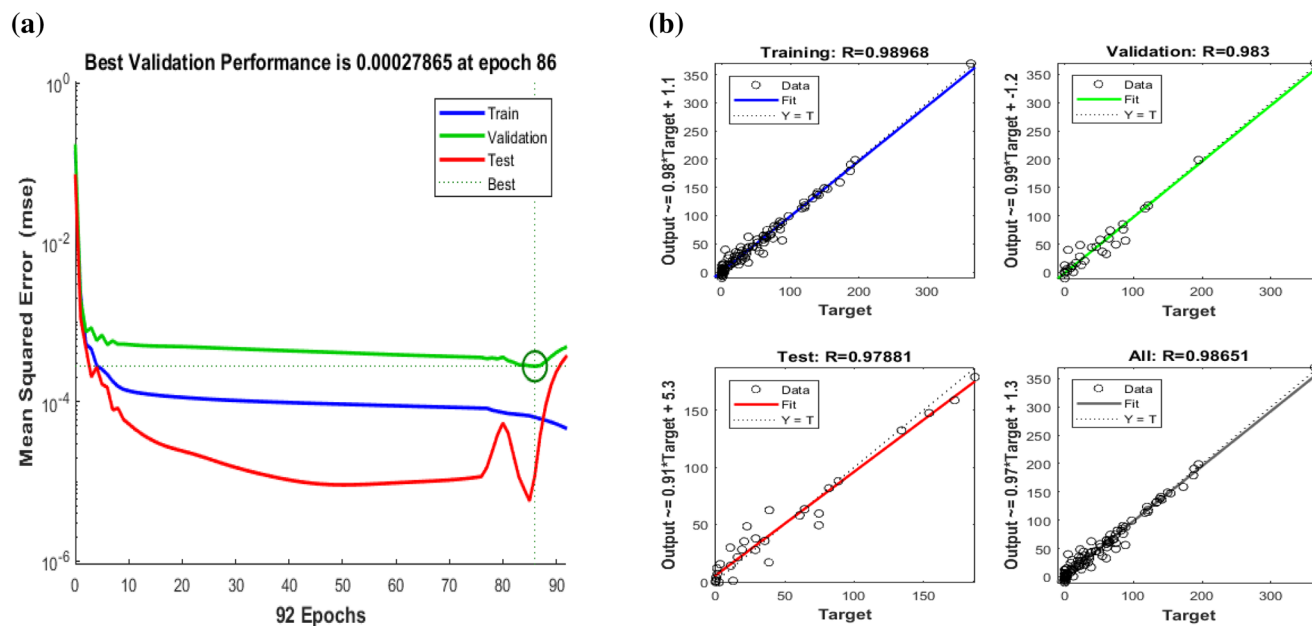


Fig. 12 Performance and regression plot of permeability ANN model

Table 6 Comparison between the developed ANN model and previous AI models

References	Method	R ²	MSE
Aminian and Ameri (2005)	ANN	0.976	Not stated
Kumar (2012)	ANN	0.87	0.0024
Yeganeh et al. (2012)	ANN	0.974	0.003
Esmailzadeh et al. (2013)	ANN	0.978	Not stated
Fegh et al. (2013)	ANN	0.84	Not stated
Iturrarán-Viveros and Parra (2014)	ANN	0.9063	0.1876
Esmailzadeh et al. (2013)	ANN	0.978	Not stated
Nguyen et al. (2014)	ANN	0.871	Not stated
Konaté et al. (2015)	GRNN	0.97	0.278
Al-Mudhafar (2017)	MLR	0.955	Not stated
Jamalian et al. (2018)	LSSVM	0.984	1.42
Zolotukhin and Gayubov (2019)	ANN	0.92	Not stated
This study	ANN	0.988	2.78×10^{-4}

probability curve. Moreover, the 3D model's distribution of porosity ranking is shown in Fig. 14b. In this illustration, the porosity models show significant difference distribution that covers over all the geological uncertainties. The plot of ranked nine representative permeability models is highlighted in Fig. 14c.

Furthermore, Fig. 14d shows the oil recovery factor for the nine different realizations simulated over a 25-year period. This highlights the geological uncertainty effect on oil recovery.

Afterwards, the nine quantiles (P10, P20, P30, ..., and P90) were adapted in the robust design for the MEOR process optimization. This high-resolution model consists of 2 million grid blocks. Therefore, it was upscaled to a simulation model with 15,000 grid cells to satisfy the CPU demand in the reservoir simulation. These geological models were later coupled with dynamic flow and physics mechanism of the microbe and substrate reaction in the reservoir simulator as described in the 1D simulation case. Figure 15 depicts the reservoir model with a five-spot line for well placement optimization purpose. The well pattern is the following specification conditions (Table 7).

The goal was to optimize the average oil recovery of the total 25 years of MEOR operation by determining the best well location and operating conditions for the four producers from 2018 to 2043. The well placement was considered to evaluate the effectiveness of the most suitable well location to enhance the microbial enhanced oil recovery under geological uncertainties.

Base case simulation results

This study focuses on EOR based upon the promotion of microbial activity that in turn generates appropriate chemicals within the reservoir. Our analysis treats only reservoir inoculation with function-specific microbes, thereby incorporating reaction engineering into reservoir engineering.

Our base case is an exogenous microbe injected and making use of in situ carbon source. As indicated by well bottom hole pressure (Fig. 16), there was improved flow

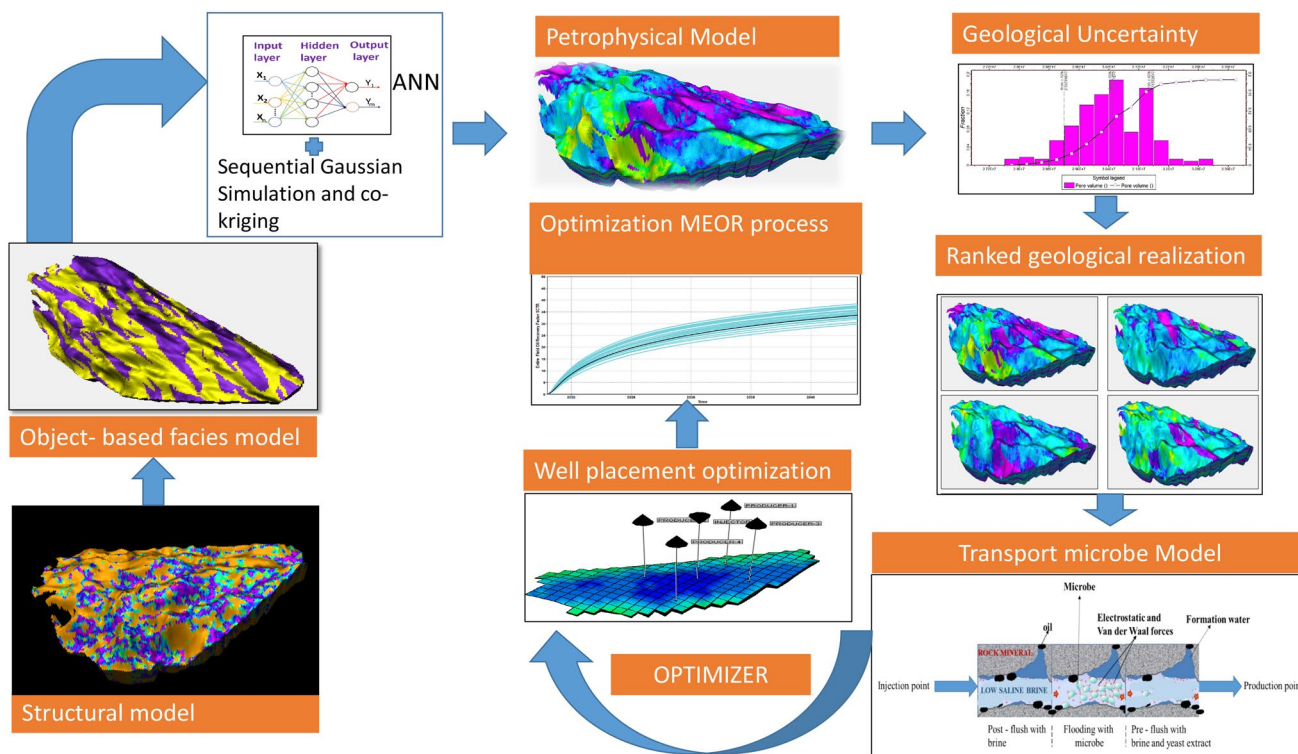


Fig. 13 Schematic of full-field model simulation and optimization

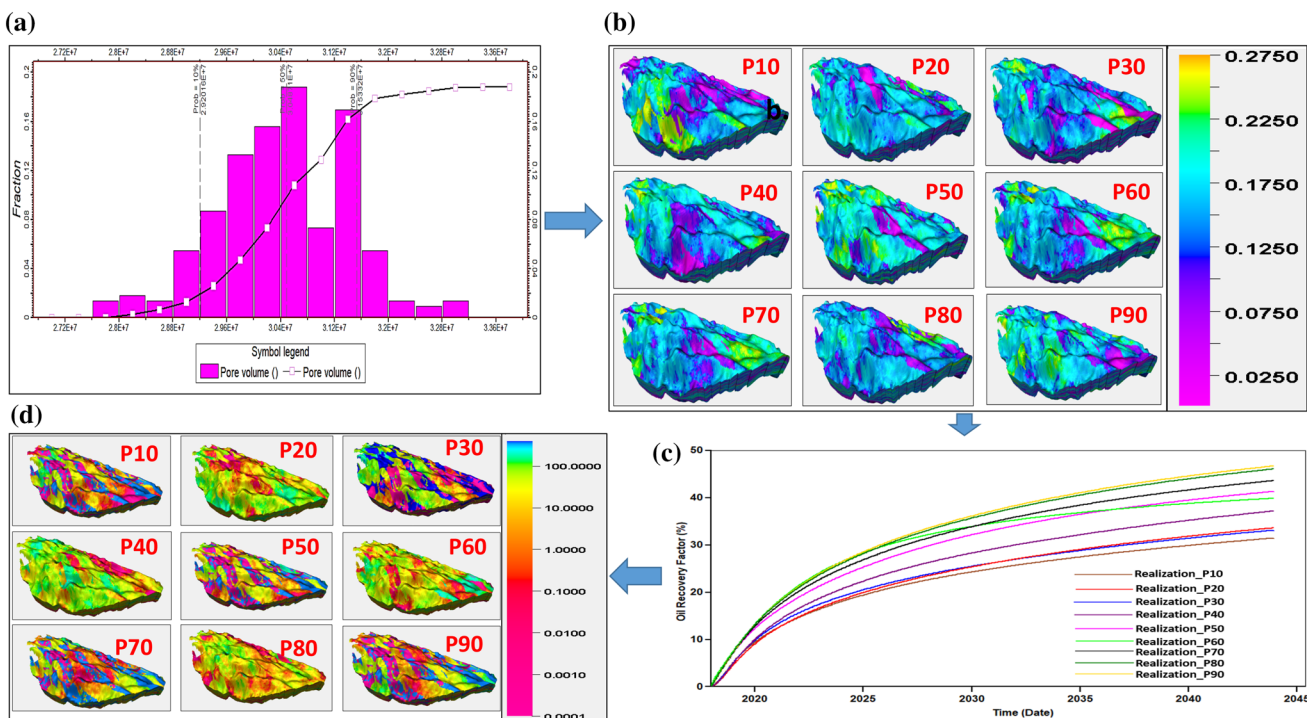


Fig. 14 a Histogram of the 200 porosity realization. b 3D models' distribution of the porosity realizations. c The nine ranked permeability models selected for optimization studies. d Oil recovery factor for the different geological realizations

conformance and increased sweep efficiency by preferential plugging of high permeable zones, thereby forcing water to produce oil from previously unswept part of the reservoir. This is highlighted by the increase in pressure at the start of the microbe injection after the pressure flattens at the end of the water flooding regime. Also, assessing the pre- and post-MEOR oil production rate (Fig. 16), we witness two main typical MEOR field responses (Segovia et al. 2009):

1. *Sweeping effect* This happens within a relatively short period of time and is characterized by a peak oil rate just after injecting microbes. This further resulted in an increase in oil production due to starting production in originally by-passed oil zones.
2. *Radial colonization* This happened at the tail end of the microbe treatment at a low oil flow rate. This prolonged MEOR effect causes a continuous oil decline rate due to metabolism (CH_4 and CO_2) as well as biodegradation of oil *n*-alkanes specifically at zones further away from colonization radius.

Figures 17 and 18 show the oil saturation map, CO_2 and CH_4 from the injection wells to the production wells, respectively. This is indicative that the microbe at the onset of injection can grow and be transported from the injection point to the production well whilst producing the needed metabolites for oil recovery. As the microbe grows, the oil saturation decreases from about 0.7 to 0.2 with time (Fig. 17), while the production of biogas increases (Fig. 18).

Table 7 Well conditions for the simulation

Pattern area	1500 m × 1000 m
Water injection rate	9000–12,000 m ³ /day
Minimum bottom hole pressure for producers	20 MPa

Role of geology in the MEOR process

Using the already generated 200 porosity and permeability realizations, we ranked these to emphasize the critical influence of geology on the MEOR process. As indicated in Fig. 19, the porosity and permeability model variations had a strong influence on the performance of the MEOR process. This plot depicts a wide range of MEOR oil recovery factors, from 28.2 to 44.9% OOIP for the various 200 realizations.

Figure 20 highlights three representative geological realizations with significant dissimilarity in the oil recovery factor. Since the well placement is the same for all realizations, the difference in the permeability distribution amongst the realizations affected the microbes' transport and subsequent interaction with nutrient during injection and transport. Also, the difference in permeability led to a change in sweep efficiency which influenced the oil recovery factor. These three realizations represent three different classes of MEOR performance, judging from their different geological makeup. The ultimate oil recovery significantly changed from realization 195 (41.6% OOIP) to realization 70 (35.1% OOIP) and to realization 32 (29.2% OOIP), respectively.

The realization number 32 had the lowest the final oil recovery factor compared with the other realizations, as per its oil saturation map (Fig. 21). The main reason is that

Fig. 15 Five-spot quarter model designed for well optimization

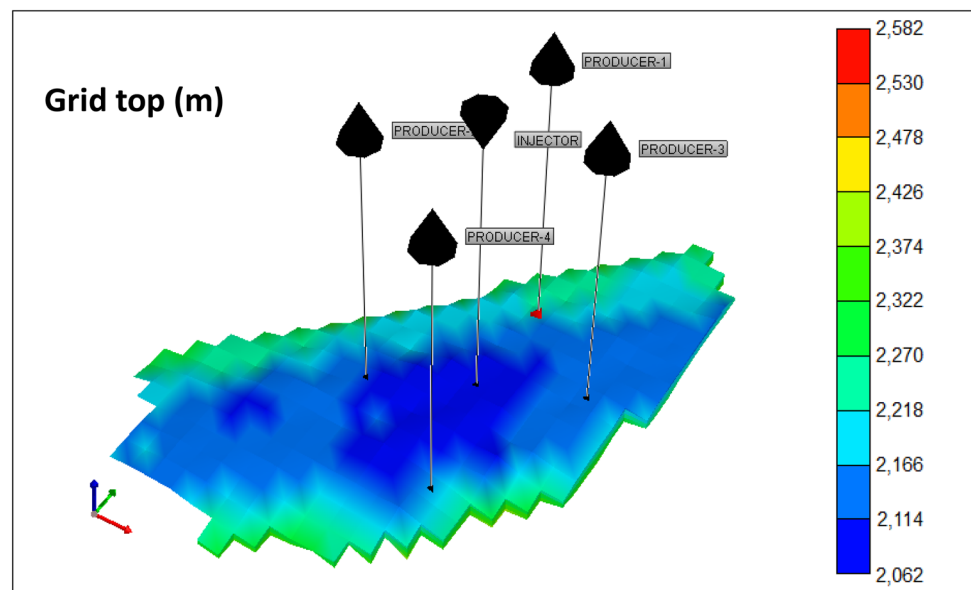


Fig. 16 Oil rate and well bottom hole pressure for MEOR flooding

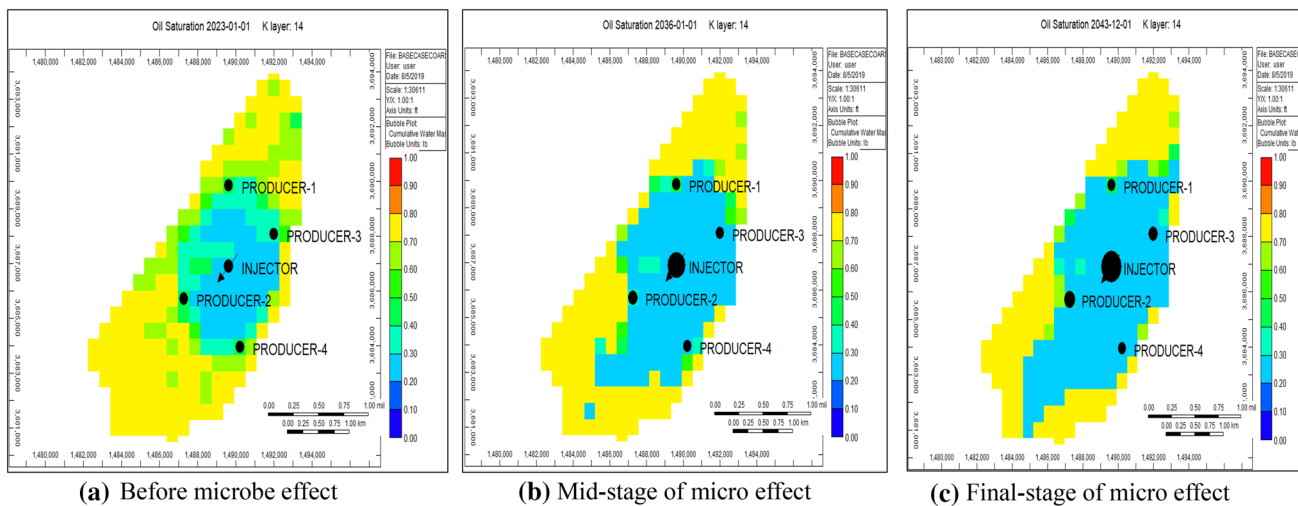
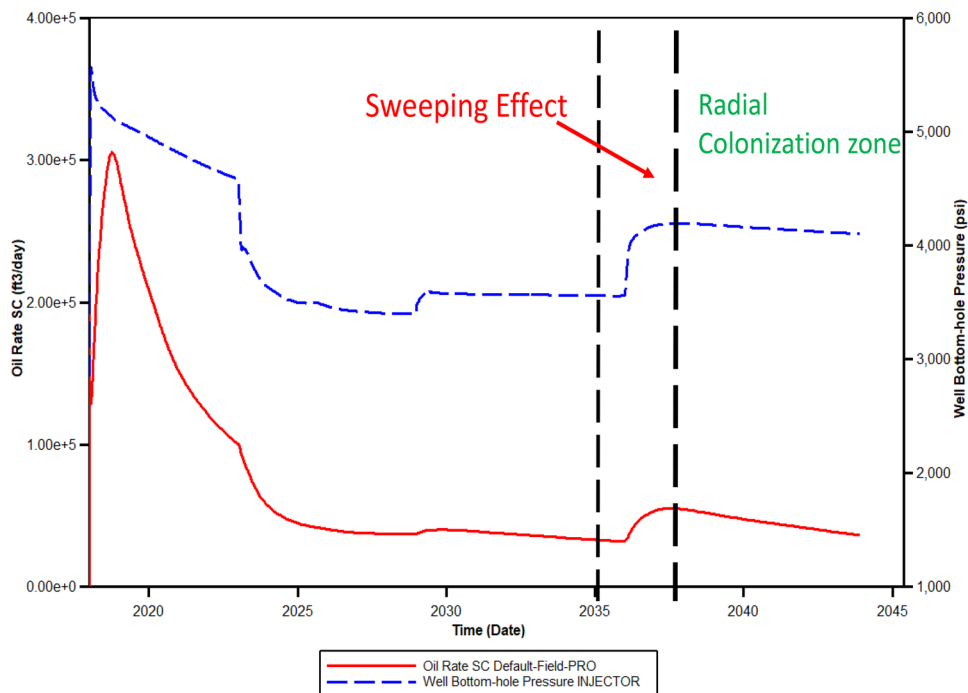


Fig. 17 Oil saturation map

the five-spot injection pattern was in a region of floodplain shale facies. Hence, resulting inflow severe associated with the injected aqueous phase through this low-porosity and low-permeability regions. This resulted in less oil displacement compared with realizations 70 and 195, as illustrated in Fig. 21. This case demonstrates that considering only the influence of injected nutrient-brine composition on MEOR without geological uncertainties is not adequate. Basically, salinity brine contact with mineral compositions should influence the microbe growth, transportation and its subsequent production of metabolites to enhance oil recovery.

However, placing an injection well in an extreme environment such as a high shale, low-porosity and low-permeability area can be detrimental to oil production and the overall success of MEOR. Therefore, well placement optimization is noted to be very necessary for any MEOR approach and should be considered during the initial field development plan for MEOR implementation.

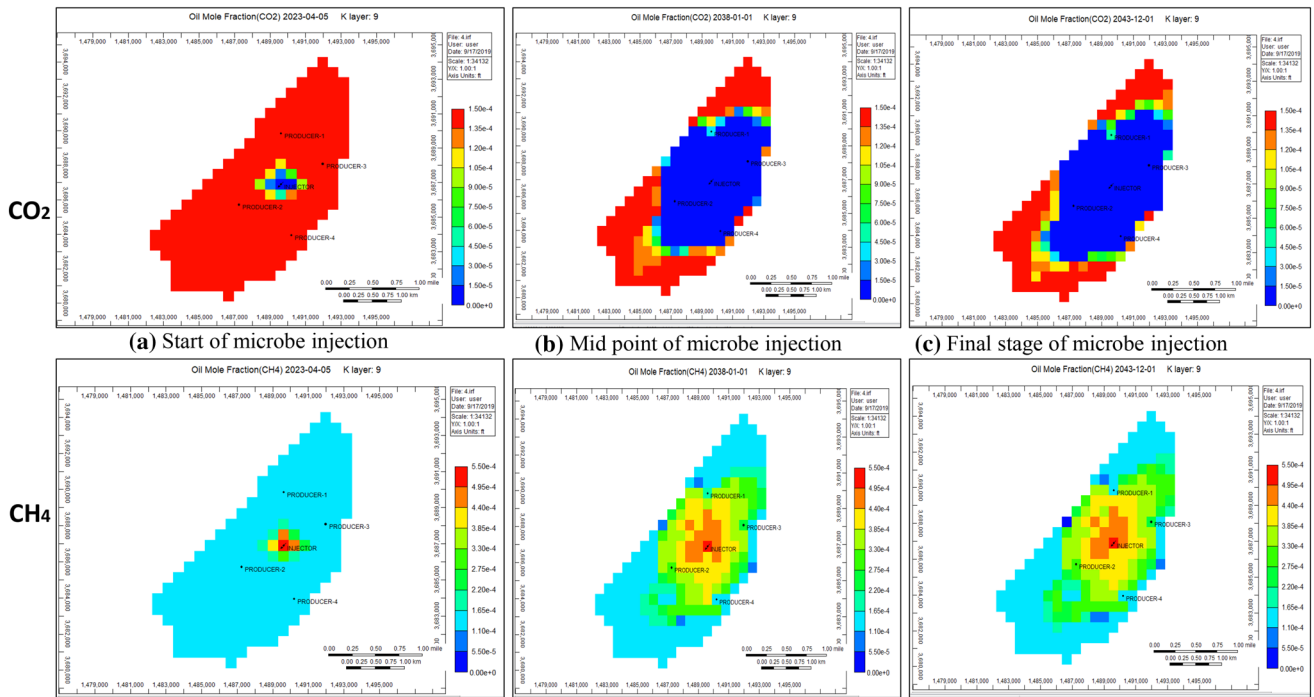


Fig. 18 CO₂ (top) and CH₄ (bottom) saturation maps

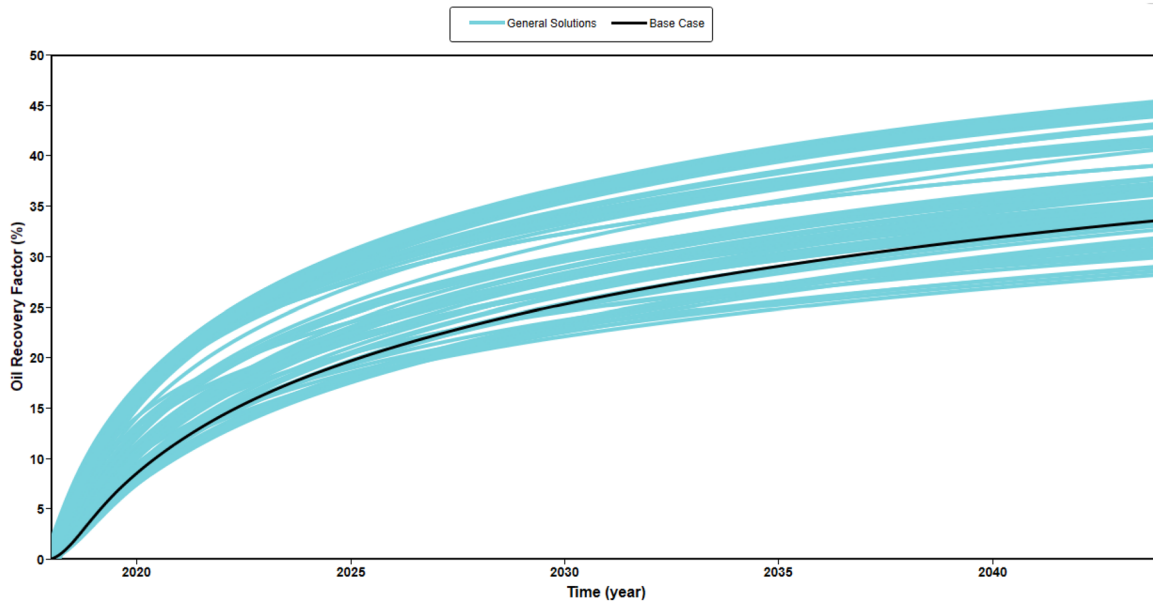


Fig. 19 Oil recovery in relation to different geological realizations

Conclusion

This study has demonstrated that through systematic simulation considering both physical and biochemical parameters, the uncertainties in predicting MEOR can be enlightened.

Simultaneous consideration for both geochemical and reservoir simulation reveals these key findings:

- This study predicted the possibility of modelling fluid viscosity variation that is induced by microbes incorporating the influence of reservoir heterogeneity.

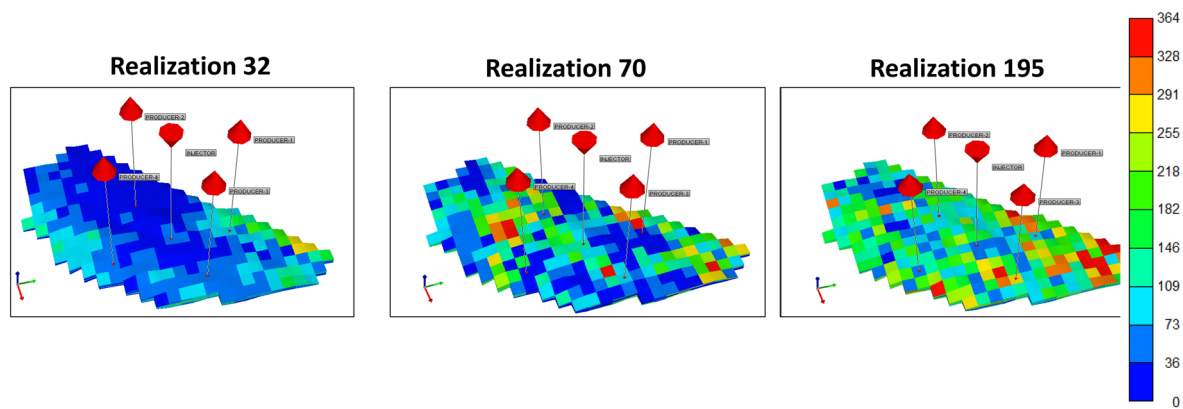


Fig. 20 Three different geological realizations selected for further analysis

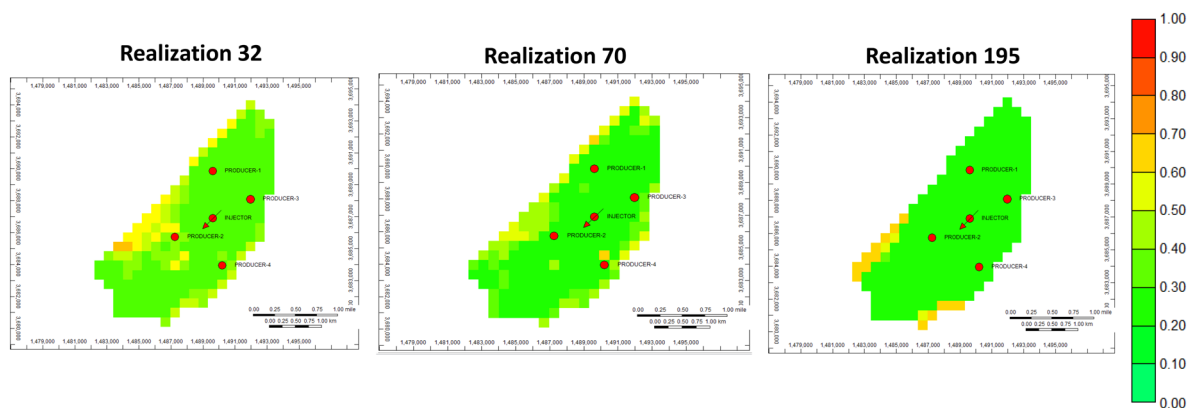


Fig. 21 Residual oil saturation maps for three selected realizations (32, 70 and 195)

- Per the core scale model: (1) MEOR can be more effective in the mixed wet core than on the water wet core; (2) water viscosity increased from 0.5 to 1.72 cP after the microbe growth and increased biomass/biofilm; and (3) by changing the stoichiometric coefficient of the components (e.g. CO_2), the viscosity of oil reduced considerably after 90 days of MEOR operation from an initial 7.1–7.07 cP and 6.40 cP, respectively.
- The challenge of upscale from laboratory- to field-scale arises from upscaling the reaction and adjusting well placement to ensure efficient transportation of the microbe from the injection to the targeted zone of recovery.
- The innovative field-scale workflow by considering multiple plausible geological models simultaneously showed that placing an injection well in an extreme environment such as a high shale, low-porosity and low-permeability area can be detrimental to oil production and the overall success of MEOR.

Acknowledgements The authors would like to extend a hand of appreciation to the Computer Modelling Group for their support towards using CMG STARS and CMOST. Also, much thankfulness to the Ministry of Education, Science and Technology (MEXT) of Japan for supporting this research. This work was financially supported by JSPS KAKENHI; Grant Number JP16K14524.

Compliance with ethical standards

Conflict of interest The authors declare that they have no conflict of interest.

Open Access This article is licensed under a Creative Commons Attribution 4.0 International License, which permits use, sharing, adaptation, distribution and reproduction in any medium or format, as long as you give appropriate credit to the original author(s) and the source, provide a link to the Creative Commons licence, and indicate if changes were made. The images or other third party material in this article are included in the article's Creative Commons licence, unless indicated otherwise in a credit line to the material. If material is not included in the article's Creative Commons licence and your intended use is not permitted by statutory regulation or exceeds the permitted use, you will need to obtain permission directly from the copyright holder. To view a copy of this licence, visit <http://creativecommons.org/licenses/by/4.0/>.

References

- Ahmadi MA (2012) Neural network based unified particle swarm optimization for prediction of asphaltene precipitation. *Fluid Phase Equilib* 314:46–51. <https://doi.org/10.1016/j.fluid.2011.10.016>
- Ahmadi MA (2015) Developing a robust surrogate model of chemical flooding based on the artificial neural network for enhanced oil recovery implications. *Math Probl Eng* 2015:1–9. <https://doi.org/10.1155/2015/706897>
- Ahmadi MA, Chen Z (2018) Comparison of machine learning methods for estimating permeability and porosity of oil reservoirs via petro-physical logs. *Petroleum*. <https://doi.org/10.1016/j.petlm.2018.06.002>
- Ahmadi MA, Chen Z (2019) Machine learning models to predict bottom hole pressure in multi-phase flow in vertical oil production wells. *Can J Chem Eng* 97:2928–2940. <https://doi.org/10.1002/cjce.23526>
- Ahmadi MA, Ebadi M (2014) Evolving smart approach for determination dew point pressure through condensate gas reservoirs. *Fuel* 117:1074–1084. <https://doi.org/10.1016/j.fuel.2013.10.010>
- Ahmadi MA, Ahmadi MR, Hosseini SM, Ebadi M (2014a) Connectionist model predicts the porosity and permeability of petroleum reservoirs by means of petro-physical logs: application of artificial intelligence. *J Pet Sci Eng* 123:183–200. <https://doi.org/10.1016/j.petrol.2014.08.026>
- Ahmadi MA, Ebadi M, Marghmaleki PS, Fouladi MM (2014b) Evolving predictive model to determine condensate-to-gas ratio in retro-graded condensate gas reservoirs. *Fuel* 124:241–257. <https://doi.org/10.1016/j.fuel.2014.01.073>
- Alkan H, Klueglein N, Mahler E, Kögler F, Beier K, Jelinek W, Herold A, Hatscher S, Leonhardt B (2016) An integrated German MEOR project, update: risk management and Huff'n Puff design. In: *SPE improved oil recovery conference*, pp 1–21. <https://doi.org/10.2118/179580-MS>
- Al-Mudhafar WJ (2017) Integrating well log interpretations for lithofacies classification and permeability modeling through advanced machine learning algorithms. *J Pet Explor Prod Technol* 7:1023–1033. <https://doi.org/10.1007/s13202-017-0360-0>
- Al-Mudhafar WJ, Rao DN, Srinivasan S (2018) Reservoir sensitivity analysis for heterogeneity and anisotropy effects quantification through the cyclic CO₂-Assisted Gravity Drainage EOR process—a case study from South Rumaila oil field. *Fuel* 221:455–468. <https://doi.org/10.1016/j.fuel.2018.02.121>
- Aminian K, Ameri S (2005) Application of artificial neural networks for reservoir characterization with limited data. *J Pet Sci Eng* 49:212–222. <https://doi.org/10.1016/j.petrol.2005.05.007>
- Ansah EO, Sugai Y, Nguere R, Sasaki K (2018a) Integrated microbial enhanced oil recovery (MEOR) simulation: main influencing parameters and uncertainty assessment. *J Pet Sci Eng*. <https://doi.org/10.1016/j.petrol.2018.08.005>
- Ansah EO, Sugai Y, Sasaki K (2018b) Modeling microbial-induced oil viscosity reduction: effect of temperature, salinity and nutrient concentration. *Pet Sci Technol*. <https://doi.org/10.1080/10916466.2018.1463253>
- Ariadji T, Astuti DI, Aditiawati P, Purwasena IA, Persada GP, Soeparmono MR, Amirudin NH, Anangadipa AA, Sasongko SY, Abqory MH, Ardianto RN, Subiantoro E, Aditya GH (2017) Microbial huff and puff project at mangunjaya field wells: the first in Indonesia towards successful MEOR implementation. In: *SPE/IATMI Asia Pacific Oil and gas conference and exhibition*. <https://doi.org/10.2118/186361-MS>
- Behesht M, Roostaazad R, Farhadpour F, Pishvaei MR (2008) Model development for MEOR process in conventional non-fractured reservoirs and investigation of physico-chemical parameter effects. *Chem Eng Technol*. <https://doi.org/10.1002/ceat.20080094>
- Bryant SL, Lockhart TP (2002) Reservoir engineering analysis of microbial enhanced oil recovery. *SPE Reserv Eval Eng*. <https://doi.org/10.2118/79719-PA>
- Bultemeier H, Alkan H, Amro M (2014) A new modeling approach to MEOR calibrated by bacterial growth and metabolite curves. *Society of Petroleum Engineers. SPE EOR Conference at Oil and Gas West Asia 2014 Driv. Integr. Innov. EOR*, pp 104–118. <https://doi.org/10.2118/169668-ms>
- Desouky SM, Abdel-Daim MM, Sayyouh MH, Dahab AS (1996) Modelling and laboratory investigation of microbial enhanced oil recovery. *J Pet Sci Eng* 15:309–320. [https://doi.org/10.1016/0920-4105\(95\)00044-5](https://doi.org/10.1016/0920-4105(95)00044-5)
- Eastcott L, Shiu WY, Mackay D (1988) Environmentally relevant physical–chemical properties of hydrocarbons: a review of data and development of simple correlations. *Pollut, Oil Chem*. [https://doi.org/10.1016/S0269-8579\(88\)80020-0](https://doi.org/10.1016/S0269-8579(88)80020-0)
- Esmailzadeh S, Afshari A, Motafakkerfard R (2013) Integrating artificial neural networks technique and geostatistical approaches for 3D geological reservoir porosity modeling with an example from one of Iran's oil fields. *Pet Sci Technol* 31:1175–1187. <https://doi.org/10.1080/10916466.2010.540617>
- Fegh A, Riahi MA, Norouzi GH (2013) Permeability prediction and construction of 3D geological model: application of neural networks and stochastic approaches in an Iranian gas reservoir. *Neural Comput Appl* 23:1763–1770. <https://doi.org/10.1007/s00521-012-1142-8>
- Goldman JC, Carpenter EJ (1974) A kinetic approach to the effect of temperature on algal growth. *Limnol Oceanogr*. <https://doi.org/10.4319/lo.1974.19.5.0756>
- Hosseini-noosheri P, Lashgari HR, Sepehrnoori K (2016) A novel method to model and characterize in situ bio-surfactant production in microbial enhanced oil recovery. *Fuel*. <https://doi.org/10.1016/j.fuel.2016.06.035>
- Islam MR, Farouq Ali SM (1990) New scaling criteria for chemical flooding experiments. *J Can Pet Technol* 29:29–36. <https://doi.org/10.2118/89-04-05>
- Iturrarán-Viveros U, Parra JO (2014) Artificial Neural Networks applied to estimate permeability, porosity and intrinsic attenuation using seismic attributes and well-log data. *J Appl Geophys* 107:45–54. <https://doi.org/10.1016/j.jappgeo.2014.05.010>
- Jamalian M, Safari H, Goodarzi M, Jamalian M (2018) Permeability prediction using artificial neural network and least square support vector machine methods. In: *80th EAGE conference and exhibition 2018*. Copenhagen, Denmark, 11–14 June. <https://doi.org/10.3997/2214-4609.201801506>
- Kaster KM, Hiorth A, Kjeilen-Eilertsen G, Boccadoro K, Lohne A, Berland H, Stavland A, Brakstad OG (2012) Mechanisms involved in microbially enhanced oil recovery. *Transp Porous Media* 91:59–79. <https://doi.org/10.1007/s11242-011-9833-7>
- Konaté AA, Pan H, Khan N, Yang JH (2015) Generalized regression and feed-forward back propagation neural networks in modelling porosity from geophysical well logs. *J Pet Explor Prod Technol* 5:157–166. <https://doi.org/10.1007/s13202-014-0137-7>
- Kumar A (2012) Artificial neural network as a tool for reservoir characterization and its application on in the petroleum engineering. In: *Offshore technology conference*. Texas, USA, 30 April–3 May. <https://doi.org/10.4043/22967-MS>
- Lazar I, Petrisor IG, Yen TF (2007) Microbial enhanced oil recovery (MEOR). *Pet Sci Technol* 25:1353–1366. <https://doi.org/10.1080/10916460701287714>
- Li J, Liu J, Trefry MG, Liu K, Park J, Haq B, Johnston CD, Clennell MB, Volk H (2012) Impact of rock heterogeneity on interactions of microbial-enhanced oil recovery processes. *Transp Porous Media* 92:373–396. <https://doi.org/10.1007/s11242-011-9908-5>

- Meckenstock RU, Von Netzer F, Stumpp C, Lueders T, Himmelberg AM, Hertkorn N, Schmitt-Kopplin P, Harir M, Hosein R, Haque S, Schulze-Makuch D (2014) Water droplets in oil are microhabitats for microbial life. *Science*. <https://doi.org/10.1126/science.1252215>
- Moosavi SR, Wood DA, Ahmadi MA, Choubineh A (2019) ANN-based prediction of laboratory-scale performance of CO₂-foam flooding for improving oil recovery. *Nat Resour Res* 28:1619–1637. <https://doi.org/10.1007/s11053-019-09459-8>
- Nguyen TBN, Bae W, Nguyen LA, Dang TQC (2014) A new method for building porosity and permeability models of a fractured granite basement reservoir. *Pet Sci Technol* 32:1886–1897. <https://doi.org/10.1080/10916466.2010.551241>
- Nielsen SM (2010) Microbial enhanced oil recovery—advanced reservoir simulation. Ph.D. Thesis. Technical University of Denmark, Kgs. Lyngby, Denmark
- Nielsen SM, Nesterov I, Shapiro AA (2016) Microbial enhanced oil recovery—a modeling study of the potential of spore-forming bacteria. *Comput Geosci* 20:567–580. <https://doi.org/10.1007/s10596-015-9526-3>
- Purwasena IA, Sugai Y, Sasaki K (2009) Estimation of the potential of an oil-viscosity-reducing bacteria, *Petrotoga* sp., isolated from an oilfield for MEOR. In: Society of Petroleum Engineers—international petroleum exhibition and conference 2009, IPTC 2009, vol 4, pp 2811–2818. <https://doi.org/10.2523/13861-MS>
- Purwasena IA, Sugai Y, Sasaki K (2014a) *Petrotoga japonica* sp. nov., a thermophilic, fermentative bacterium isolated from Yabase Oilfield in Japan. *Arch Microbiol* 196:313–321. <https://doi.org/10.1007/s00203-014-0972-4>
- Purwasena IA, Sugai Y, Sasaki K (2014b) Estimation of the potential of an anaerobic thermophilic oil-degrading bacterium as a candidate for MEOR. *J Pet Explor Prod Technol* 4:189–200. <https://doi.org/10.1007/s13202-013-0095-5>
- Saito M, Sugai Y, Sasaki K, Okamoto Y, Ouyang C (2016) Experimental and numerical studies on EOR using a biosurfactant. *Abu Dhabi Int Pet Exhib Conf* 1:1–11. <https://doi.org/10.2118/183496-MS>
- Segovia GC, Huerta VA, Ypf R, Gutierrez GC, Energia P (2009) SPE 123072 improving MEOR performance by a selection methodology in mature oilfields
- Shabani-Afrapoli M, Li S, Alipour S, Torsater O (2011) Experimental and numerical study of microbial improved oil recovery in a pore scale model by using COMSOL. In: Proceedings of the 2011 COMSOL conference on Stuttgart
- Shabani-Afrapoli M, Crescente C, Li S, Alipour S, Torsater O (2012) Simulation study of displacement mechanisms in microbial improved oil recovery experiments. In: Society of Petroleum Engineers—SPE EOR conference at Oil Gas West Asia 2012, OGWA—EOR: building towards sustainable growth, vol 1. <https://doi.org/10.2118/153323-MS>
- Spirov P, Ivanova Y, Rudyk S (2014) Modelling of microbial enhanced oil recovery application using anaerobic gas-producing bacteria. *Pet Sci* 11:272–278. <https://doi.org/10.1007/s12182-014-0340-7>
- Sugai Y, Hong C, Chida T, Enomoto H (2007) Simulation studies on the mechanisms and performances of MEOR using polymer producing microorganism. *Asia Pacific Oil Gas Conf Exhib, Proc*. <https://doi.org/10.2118/110173-MS>
- Sugai Y, Komatsu K, Sasaki K, Mogensen K, Bennetzen MV (2014) Microbial-induced oil viscosity reduction by selective degradation of long-chain alkanes. In: Society of Petroleum Engineers—30th Abu Dhabi international petroleum exhibition and conference ADIPEC 2014 challenges and opportunities for the next 30 years, vol 3, pp 1–13
- Thrasher D, Puckett DA, Davies A, Beattie G, Pospisil G, Boccardo G, Vance I, Jackson S, Alaska BP (2010) MEOR [microbial enhanced oil recovery] from lab to field. In: 17th SPE improved oil recovery symposium [IOR] (Tulsa, OK, 4/24–28/2010) Proceedings
- Vo Thanh H, Sugai Y, Nguele R, Sasaki K (2019a) Integrated work flow in 3D geological model construction for evaluation of CO₂ storage capacity of a fractured basement reservoir in Cuu Long Basin, Vietnam. *Int J Greenh Gas Control* 90:102826. <https://doi.org/10.1016/j.ijggc.2019.102826>
- Vo Thanh H, Sugai Y, Sasaki K (2019b) Impact of a new geological modelling method on the enhancement of the CO₂ storage assessment of E sequence of Nam Ung field, offshore Vietnam. *Energy Sources Part A Recover Util Environ Eff*. <https://doi.org/10.1080/15567036.2019.1604865>
- Vo Thanh H, Sugai Y, Nguele R, Sasaki K (2020) Robust optimization of CO₂ sequestration through a water alternating gas process under geological uncertainties in Cuu Long Basin, Vietnam. *J Nat Gas Sci Eng*. <https://doi.org/10.1016/j.jngse.2020.103208>
- Widdel F, Grundmann O (2010) Biochemistry of the anaerobic degradation of non-methane alkanes. In: Handbook of hydrocarbon and lipid microbiology. https://doi.org/10.1007/978-3-540-77587-4_64
- Wilhelm E, Battino R, Wilcock RJ (1977) Low-pressure solubility of gases in liquid water. *Chem Rev*. <https://doi.org/10.1021/cr60306a003>
- Gianetto MR (1999) Microbial enhanced oil recovery mathematical modelling and scaling up of microbial enhanced oil recovery. South Dakota School of Mines and Technology Emertec Developments Inc. V
- Yang C, Card C, Nghiem L, Fedutenko E (2011) Robust optimization of SAGD operations under geological uncertainties. In: SPE reservoir simulation symposium, pp 21–23. <https://doi.org/10.2118/141676-MS>
- Yeganeh M, Masihi M, Fathollahi S (2012) The estimation of formation permeability in a carbonate reservoir using an artificial neural network. *Pet Sci Technol* 30:1021–1030. <https://doi.org/10.1080/10916466.2010.490805>
- Zhang X, Knapp RM, McInerney MJ (1993) A mathematical model for microbially enhanced oil recovery process. *Dev Pet Sci*. [https://doi.org/10.1016/S0376-7361\(09\)70060-3](https://doi.org/10.1016/S0376-7361(09)70060-3)
- Zolotukhin AB, Gayubov AT (2019) Machine learning in reservoir permeability prediction and modelling of fluid flow in porous media. *IOP Conf Ser Mater Sci Eng* 700:012023. <https://doi.org/10.1088/1757-899X/700/1/012023>

Publisher's Note Springer Nature remains neutral with regard to jurisdictional claims in published maps and institutional affiliations.